

**DESIGN AND DEVELOPMENT OF A 10KHZ-1MHZ AC
MAGNETIC SUSCEPTOMETER**

By

Javier Tafur-Bermúdez

A thesis submitted in partial fulfillment of the requirements for the degree of

MASTER OF SCIENCE

in

ELECTRICAL ENGINEERING

UNIVERSITY OF PUERTO RICO
MAYAGÜEZ CAMPUS

November, 2011

Approved by:

José Rosado, Ph.D
Member, Graduate Committee

Date

Carlos Rinaldi, Ph.D
Member, Graduate Committee

Date

Eduardo Juan-García, Ph.D
President, Graduate Committee

Date

Rubén E. Díaz-Rivera, Ph.D
Representative of Graduate Studies

Date

Pedro I. Rivera-Vega, Ph.D
Chairperson of the Department

Date

Abstract of Thesis Presented to the Graduate School
of the University of Puerto Rico in Partial Fulfillment of the
Requirements for the Degree of Master of Science

**DESIGN AND DEVELOPMENT OF A 10KHZ-1MHZ AC
MAGNETIC SUSCEPTOMETER**

By

Javier Tafur-Bermúdez

November 2011

Chair: Eduardo Juan-García

Major Department: Electrical and Computer Engineering

Development and improvement of instruments used to characterize magnetic materials is one of the most important tasks in science, which could lead to relevant studies in material science and engineering. The AC magnetic susceptometer is an instrument which consists in a coil arrangement used to investigate magnetic properties such as magnetic susceptibility. Current AC susceptometer design present a limited frequency range, commonly up to 10kHz, preventing the study of magnetic properties dependence on magnetic field frequency, which is crucial in investigations such as specific absorption rate of nanoparticles used for hyperthermia treatment. For this reason, the design and development of a frequency improved AC susceptometer operating from 10 kHz to 1MHz with a constant excitation field of approximately 4.25 Oe is of interest. Some considerations such as wire selection to avoid parasitic capacitances between the turns and sensing bridge electronics were further developed in order to extend the operating frequency range. A high speed instrumentation amplifier with a slew rate over $33V/\mu s$ was designed and constructed

using voltage feedback LM7171 operational amplifiers. The AC susceptometer operation in the 10 kHz-1MHz frequency range was validated by measuring the complex magnetic susceptibility of cobalt ferrite nanoparticles suspended in different mixtures of mineral oil and hexane. The viscosity of the solvents were obtained from the Brownian relaxation time equation and compared with the viscosities obtained from a validated instrument. Results were in good agreement with the theoretical Debye model.

Resumen de Tesis Presentado a Escuela Graduada
de la Universidad de Puerto Rico como requisito parcial de los
Requerimientos para el grado de Maestría en Ciencias

**DISEÑO Y DESARROLLO DE UN SUSCEPTÓMETRO
MAGNÉTICO AC CON UN RANGO DE FRECUENCIA DE
10KHZ-1MHZ**

Por

Javier Tafur-Bermúdez

Noviembre 2011

Consejero: Eduardo Juan-García

Departamento: Ingeniería Eléctrica y Computadoras

El desarrollo de instrumentos para caracterizar materiales magnéticos es una de las labores mas importantes en las ciencias, el cual puede llevar a estudios relevantes en las ciencias de materiales e ingeniería. El susceptómetro magnético AC es un instrumento que consiste de un arreglo de embobinados el cual es usado para investigar las propiedades magnéticas de los materiales tal como la susceptibilidad magnética. Los susceptómetros AC que se han desarrollado actualmente presentan un rango limitado de frecuencia que llega comunmente hasta 10kHz, lo cual evita el estudio sobre la dependencia de frecuencia de las propiedades magnéticas, siendo esto crucial en estudios tales como la razón de absorción específica de la nanoparticulas que se usan para hipertermia. Por esta razón se interesa diseñar y desarrollar un susceptómetro AC con un rango de frecuencia mejorado que opere desde 10kHz hasta 1MHz con un campo de excitación constante de 4.25 Oe. Algunas consideraciones tales como la selección de cable para evitar las capacitancias parasíticas que

existen entre los cables de los embobinados y el circuito de medición fueron desarrolladas con el propósito de extender el rango de operación de frecuencia. Un amplificador de instrumentación de alta velocidad con un "slew rate" mayor de $33\text{V}/\mu\text{s}$ fue diseñado y construido usando el amplificador operacional de retroalimentación de voltaje LM7171. La operación del susceptómetro AC en el rango de frecuencia de 10kHz - 1MHz fue validada a través de las medidas de susceptibilidad magnética compleja de nanopartículas de ferrita de cobalto suspendidas en diferentes mezclas de aceite mineral con hexano. Las viscosidades de los solventes fueron obtenidas a través de la ecuación de relajación Browniana y comparadas con la viscosidad obtenidas de un instrumento validado. Los resultados fueron acordes con el modelo teórico de Debye.

ACKNOWLEDGMENTS

I would like to thank my advisor Prof. Eduardo Juan for his academical support and guidance, and for giving me the opportunity of being member of the Biomedical Instrumentation Research Laboratory (BIRLab) all these years.

Also, I would like to thank the members of my committee, Prof. Carlos Rinaldi for the academic support and guidance, and for giving me the opportunity of working in the Chemical Engineering Laboratory, and being part of my thesis committee, and Prof. José Rosado for recommendations, advice, and being interested in being part of my thesis committee.

I would like to thank the professors of the Electronics program for giving me the opportunity of working in their laboratories, let me use the laboratory instruments, recommendations, and mentorship.

Finally, special thanks to my BIRLab friends for all their support and funny times. Special thanks to my friends of chemical engineering for answering my questions about chemistry, knowledge sharing, and accepting me as a member of their group. Also, special thanks to my family, including the Highland group and school friends, for all their understanding and unconditional support.

This work was supported by the National Science Foundation under grant HRD-0833117.

TABLE OF CONTENTS

	<u>page</u>
ABSTRACT	ii
RESUMEN	iv
ACKNOWLEDGMENTS	vi
LIST OF FIGURES	ix
LIST OF ABBREVIATIONS	xiii
LIST OF SYMBOLS	xiv
1 Introduction	1
1.1 AC Susceptometer Designs and Developments	1
1.2 Brief summary of magnetic fluids application on determining fluid viscosity	4
1.3 Motivation	8
1.4 Objectives	8
1.5 Outline	9
2 Theoretical Background	11
2.1 Electromagnetism	11
2.1.1 Relationship between magnetic field and current	11
2.1.2 Magnetic force and magnetic dipole moment	13
2.1.3 Magnetic materials	14
2.2 Fluid Mechanics	20
2.2.1 Fluid Properties	20
2.2.2 Magnetic fluids	23
3 Experimental Procedure	29
3.1 AC susceptometer design	29
3.1.1 System Development	31
3.1.2 Setup Procedure	36
3.2 FERROFLUIDS	38
3.2.1 Particle synthesis and characterization	38
4 Results	41
4.1 Data and analysis of complex magnetic susceptibility	41

4.2	Viscosity measurements and comparison with values obtained from complex magnetic susceptibility	44
4.3	Discussion	45
5	Conclusion and Recommendations	47
A	Derivation of Equations	49
A.1	Mathematical description of the generation of a magnetic field and the magnetic field intensity at any point of a non-infinite coil [2]	49
A.2	Output voltage of a secondary coil with a symmetric first-order gradiometer configuration	50
B	Summary of LabVIEW operation	54

LIST OF FIGURES

<u>Figure</u>	<u>page</u>
1-1 A commercial AC susceptometer: Imego Dynamag AC susceptometer [3]	1
1-2 a) Symmetric first-order gradiometer b) Second-order Gradiometer c) Asymmetric Gradiometer d) Concentric Gradiometer e) Planar Gradiometer [10]	2
1-3 Dynamic response of some ferrofluids magnetization considering the Debye model for dipolar systems	6
2-1 Magnetic moment generated by a positively charged particle. A mag- netic field at point P is generated by the current loop	14
2-2 Schematic of single crystal or monocrystalline, polycrystalline, and amorphous material structures [39]	15
2-3 Behaviour of isotropic and anisotropic materials, in where variable E represents the Young Modulus. This figure shows that the stress in response to a strain varies with direction[40]	17
2-4 Atomic dipole configuration for a diamagnetic material [37]	17
2-5 Atomic dipole configuration for a paramagnetic material [37]	18
2-6 Magnetization curves of vacuum, diamagnetic and paramagnetic ma- terial [41]	18
2-7 a) Typical hysteresis magnetization curves, with a saturation S, a remanence R and a coercive form H_c . b) Magnetic flux density (B) versus magnetic field intensity (H) behavior for ferromagnetic and ferrimagnetic materials, in where is presented the material with initial permeability μ_i , and whose domain adopt different con- figurations during several stages of magnetization until it reaches saturation.[37]	19
2-8 Ordering of the atomic dipoles in a) ferromagnetic and b) ferrimag- netic material [37]	20

2-9	Comparison of the shear stress vs shear rate behavior in one Newtonian fluid, such as water, and two non-Newtonian fluids, such as the dilatants and the pseudoplastic fluids. Dilatants increase in apparent viscosity at higher shear rates, different from pseudoplastic fluids that have a lower apparent viscosity at higher shear rates. An example of dilatants and pseudoplastic fluids are printing inks and starch solution, respectively.[47] Another non-Newtonian material not strictly a liquid is the Bingham plastic, which is a viscoplastic material that behaves as a rigid body at low stresses but flows as a viscous fluid at high stress.[48]	22
3-1	Diagram of the AC susceptometer configuration. The input sinusoidal signal is amplified to enhance the magnetic field which decreases at higher frequencies due to the inductive impedance of the primary. A first order gradiometer as secondary coil senses the magnetization of the sample due to the applied AC magnetic field. The differential signal detected by the INamp is compared with the current source signal, measured from the resistor voltage, for phase-shifts and amplitude variations.	29
3-2	Picture of the coils. A Carol A 18 AWG wire was used for the primary and secondary coils.	32
3-3	Instrumentation amplifier constructed with three LM7171. Input-lag compensation was added to the two op-amps at the input to obtain stability. As well, a capacitor were added to the differential op-amp. For this application adding a resistor to obtain input-lag compensation compromises stability. All resistors have fixed values except Rg which is variable.	33
3-4	Picture of the instrumentation amplifier. Due to the unwanted internal input impedance of the multiplexer, relays are used to changes between several gain resistors (Rg), which is the resistor establishing the gain. The relays are controlled with a multiplexer, which is controlled with the computer by parallel port. At the right, an anti-aliasing 6 th order low-pass filter, which is currently in progress for future system optimization.	34
3-5	Gain vs frequency plot (left) and phase vs frequency plot (right) for the instrumentation amplifier constructed with LM7171. A small overshoot-like signal caused by the capacitor added in the differential stage is observed between 500 kHz and 800 kHz.	35
3-6	Complete AC susceptometer equipment at laboratory facility.	35
3-7	Gain and phase AC susceptometer calibration with Dy ₂ O ₃ at maximum instrumentation amplifier gain of approximately G=800V/V	37

3-8	Transmission Electron Microscope (TEM) of cobalt ferrite nanoparticles. A size and narrow size distribution of about 14.0 ± 2.0 nm was obtained.	39
3-9	Dynamic Light Scattering (DLS) of cobalt ferrite ferrofluid. A mean hydrodynamic diameter of 23.1nm is observed in three different analysis. The intensity measurement, which is commonly used to report the size of each peak in the distribution, shows two groups of nanoparticles sizes, where a group with an approximately size of 170nm has a magnitude similar to those with a size of 23.1nm.	40
3-10	Magnetization versus magnetic field for $CoFe_2O_4$ nanoparticles suspended in hexane with a concentration of 15%w/w. The initial magnetic susceptibility was 1.35×10^5 as determined from the slope at the linear region.	40
4-1	Complex magnetic susceptibility of the cobalt ferrite nanoparticles suspended in hexane. The maximum value of χ'' is observed at a frequency of $f = 65$ kHz.	41
4-2	Complex magnetic susceptibility of the cobalt ferrite nanoparticles suspended in a mixture of 75%w/w hexane-25%w/w mineral oil. The maximum value of χ'' is observed at a frequency of $f = 35$ kHz.	42
4-3	Complex magnetic susceptibility of the cobalt ferrite nanoparticles suspended in a mixture of 50%w/w hexane-50%w/w mineral oil. The maximum value of χ'' is observed at a frequency of $f = 15$ kHz.	43
4-4	Complex magnetic susceptibility of the cobalt ferrite nanoparticles suspended in a mixture of 25%w/w hexane-75%w/w mineral oil. The maximum value of χ'' cannot be observed precisely, but exists below $f = 10$ kHz.	43
4-5	Complex magnetic susceptibility of the cobalt ferrite nanoparticles suspended in mixtures of 25%w/w hexane-75%w/w mineral oil, 50%w/w hexane-50%w/w mineral oil, 75%w/w hexane-25%w/w mineral oil, 100%w/w hexane. It can be observed that maximum value for χ'' varies to higher frequencies as the viscosity of carrier fluid decreases.	44
A-1	Diagram of a current loop generating a magnetic field used as a representation of the Biot-Savart's law	49
A-2	Magnetic field intensity inside the central axis of a coil	50
A-3	Diagram of a primary and secondary coil configuration. The sample is assumed to exist in the lower coil of the secondary.	50

B-1	Program to setup the magnetic field intensity	54
B-2	Oscilloscope setup and data acquisition program	55
B-3	Program to select the waveform used to obtain the in-phase and out- of-phase values	56
B-4	Program to move the motor	57

LIST OF ABBREVIATIONS

TEM	Transmission electron microscopy.
$CoFe_2O_4$	Cobalt ferrite.
SQUID	Superconducting Quantum Interference Devices
DLS	Dynamic Light Scattering
TGA	Thermogravimetric analysis
INamp	Instrumentation amplifier
PCB	Printed Circuit Board
opamps	Operational amplifiers
AWG	American Wire Gauge
MnO	Manganese oxide

LIST OF SYMBOLS

Ψ	Magnetic flux.
τ	Relaxation time.
μ	Permeability.
μ_0	Vacuum permeability.
χ	Magnetic susceptibility.
ω	Angular frequency.
Ω	Magnetic field angular frequency.
η	Viscosity
η_0	Carrier fluid viscosity
$\dot{\gamma}$	Rate of shear deformation or shear strain rate
τ_s	Shear stress
ε	Deformation or stress
σ_Y	Tensile stress
Y or E	Young modulus or elastic modulus
t	Time
ϕ_v	Volume fractions
r_p	Radius of a spherical particle
M	Magnetization
τ_q	Torque
m	Magnetic moment
H	Intensity of magnetic field
θ	Angle
V	Volume of the magnetic particle in a fluid
τ_B	Brownian relaxation time
τ_N	Nèel relaxation time
N	Number of turns in coil
V_0	Output voltage
l	Length

CHAPTER 1

INTRODUCTION

This chapter presents a brief introduction to previous work in the design and improvement of AC susceptometers, in which is highlighted the importance of the AC susceptometers development in order to increase and improve its diverse applications. In addition, a brief introduction to ferrofluids and some of their principal applications is presented. Details of concepts meaning and mathematical description are left to Chapter 3. Finally, the motivation and the objectives are established.

1.1 AC Susceptometer Designs and Developments

AC magnetic measurements provide important characteristics of magnetic materials. Such measurements are obtained by applying an AC magnetic field to a sample whose moment is time-dependent, inducing changes in the material which yield information that cannot be obtained from DC measurements, such as for magnetization dynamics. A widely used instrument for such measurement is the AC susceptometer.[1] Figure 1-1 presents a commercial AC susceptometer.

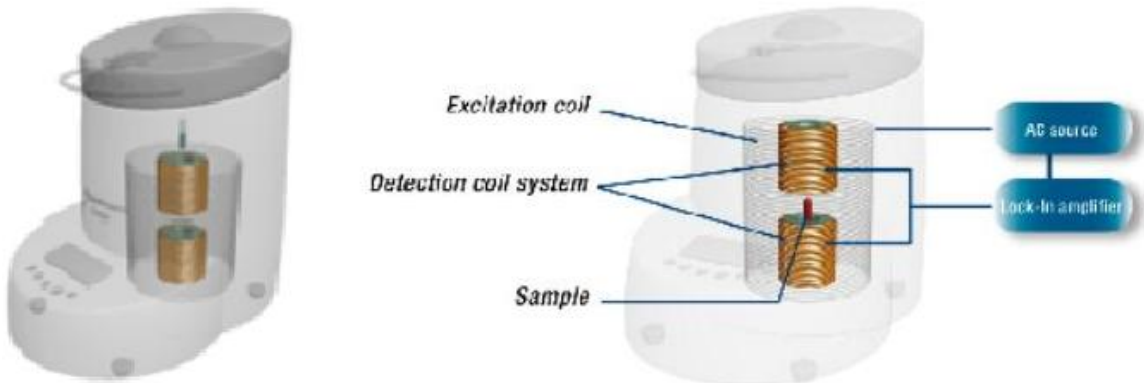


Figure 1–1: A commercial AC susceptometer: Imego Dynamag AC susceptometer [3]

The AC susceptometer is an electromagnetic instrument which could be used to measure the materials AC magnetic susceptibility. The AC magnetic susceptibility is defined in Sadiku [2] as the sensitivity of a material to respond to an applied magnetic field. The common method of measuring AC magnetic susceptibility involves a mutual inductance bridge, which was initially introduced by Hartshorn in 1925 [4]. Thereafter, several AC susceptometers based in mutual inductance bridges have been reported [5], such as in E. Maxwell 1965 [6], A.C. Anderson 1968 [7] and A.C.Anderson et al 1970 [8]. The principle of mutual inductance is based on a time-varying current flowing through a first conductive contour, which generates a time-varying magnetic field as well as a time-varying electric field, and induces an electromotive force (emf) in a second conductive contour [9]. If such contours are extended to several turns, it will be analogous to a time-varying voltage generated in a secondary coil through the induction of a time-varying magnetic field created by a time-varying current in a primary coil. The secondary coil, which for this application is also called the pickup coil or detection coil, could have several configurations depending on how much sensitivity and noise rejection is desired. These configurations measure the gradient of the magnetic field. Figure 1-2 shows several configuration for two main gradiometers, axial and planar.

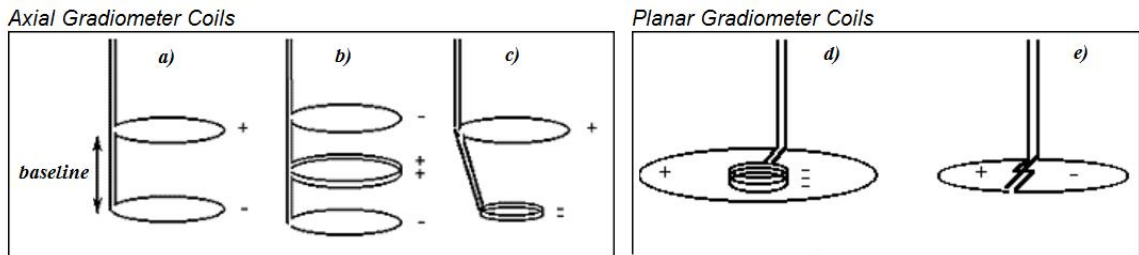


Figure 1–2: a) Symmetric first-order gradiometer b) Second-order Gradiometer c) Asymmetric Gradiometer d) Concentric Gradiometer e) Planar Gradiometer [10]

Each configuration provides a feature for specific applications such as measurements that require reasonable noise rejection and sensitivity, in which the symmetric first-order gradiometer is a good option. Depending on the the kind of measurement,

secondary coil design should be modified. For example, a better noise rejection could be achieved by the second order gradiometer, although the complexity of its arrangement needs the sample to be closer to achieve good sensitivity. A third axial gradiometer coil, the asymmetric gradiometer, could be designed to make measurements with good sensitivity and reasonable noise rejection. For applications with planar geometry, a concentric gradiometer and a planar gradiometer could be developed to obtain good sensitivity and excellent spatial resolution, respectively.[10]

The most commonly used configuration is the first-order gradiometer. The upper and lower turns are symmetric and wound in opposition, allowing the measurement of the differential voltage induced in the coil when a specimen is placed inside any of the two, upper or lower, secondary turns. Because of the simplicity of the coil arrangement, the first-order gradiometer is a very common configuration in commercial instruments. In this arrangement, assuming that the sample is of the same size as the secondary inner coil volume, its sensitivity and frequency range of work will depend on both, the number of turns and the type of wire. Similar consideration must be taken in designing the excitation coil, in which for a constant source voltage, the magnetic field intensity in a frequency sweep will depend on the number of turns and wire type.

The coil design in commercial mutual inductance susceptometers work very precisely at very low frequencies, but are limited in maintaining a constant excitation field at higher frequencies, or in measuring the induced voltage in a high frequency range because of the secondary design or the sensing bridge. Some innovative techniques have been developed to achieve measurements of complex magnetic susceptibility in a wide frequency range of 10Hz-3GHz [11] and 100MHz-16GHz [12]. Such results were obtained by using the impedance response of a ferrofluid inserted in the slit of a toroidal coil [13] or by analyzing the change of permeability in a coaxial cell of short-circuit (S/C) and open-circuit transmission line techniques [14]. Others

make use of a magneto-optic properties of the ferrofluids to obtain the carrier fluid viscosity [15] and the complex magnetic susceptibility [16] of a ferrofluid.

Although the impressive frequency ranges obtained by the transmission line and toroidal method are impressive, the mutual inductance AC susceptometers [17] offer the possibility of homogenous excitation field [18], accessibility to measure magnetic fluids as well as solids, reasonable quantity of sample and magnetic material concentration, the variety of designs [19] and applications due to sizing [20], and its well-investigated coupling with SQUIDS for high sensitivity [22][21].

Considering the relevance of the AC susceptometer in determining the properties of the material such as the complex magnetic susceptibility as a function of frequency, this work presents the design of a mutual inductance AC susceptometer with a constant excitation field of 4.25Oe from 10 kHz up to 1MHz. Instrument validation by measuring the complex magnetic susceptibility of nanoparticles and by comparing the viscosity values obtained from theoretical models and from the experimental complex magnetic susceptibility will be better understood through the ferrofluids summary presented in next section

1.2 Brief summary of magnetic fluids application on determining fluid viscosity

Recent researches are focused in the development of new nanomaterials, with dimensions typically less than 100nm, such as the emergent investigations of colloidal ferrofluids, also called magnetic fluids. A magnetic ferrofluid consists of a stable colloidal dispersion of single-domain magnetic particles in a liquid carrier. Typically, these particles are spherical with diameters between 20-100nm and are composed of ferrites, such as cobalt ferrite and magnetite, among others.

Ferrofluids provide electromagnetic and thermodynamic properties suitable for applications in the different branches of biology, chemistry and physics. In the biomedical engineering field they can be used in biosensors [23], hyperthermia [24],

drug delivery [25] and magnetic manipulation of cells [26]. Also, in other engineering field, they are used in applications such as magnetorheological dampers [27], ferrofluidic sealers [28] and heat transfer fluids [29].

Some equations could be used to describe and predict the ferrofluid's properties determined by the synthesis, such as their electrical, magnetic, rheological and thermal properties. A very important relationship commonly used is the Debye model which describes the magnetic susceptibility of the suspension in terms of the magnetic field angular frequency and the relaxation time of the particles. The magnetic susceptibility is the degree of magnetization of a magnetic material when a magnetic field is applied [30]. Such property is of crucial interest in ferrofluid research because of the existence of a complex magnetic susceptibility, as in magnetite and cobalt ferrite.

The complex magnetic susceptibility of a ferrofluid is an important parameter that can be used to characterize magnetic colloids in an accurate way. For example, the complex magnetic susceptibility of ferrofluids could be used to determine the relaxation mechanism, ferromagnetic resonance, stochastic resonance, non-linear properties, magnetic losses and the signal-to-noise ratio [31]. The real part χ' and imaginary part χ'' are related to the magnetic field energy storage and power dissipation, respectively [32]. The behavior of the complex magnetic susceptibility curves, best described by the magnetic susceptibility components of the Debye Model, depends on the frequency of the applied magnetic field. Figure 1-3 presents an illustration of the ideal behavior of the complex magnetic susceptibility in a frequency sweep.

As seen from Figure 1-3, χ'' has a maximum value at a specific frequency, and depends on the viscosity of the nanoparticles carrier fluid. Finding the frequency value in which this maximum exists, allows the possibility to determine the relaxation time of the particles. This relaxation time is mainly influenced by two

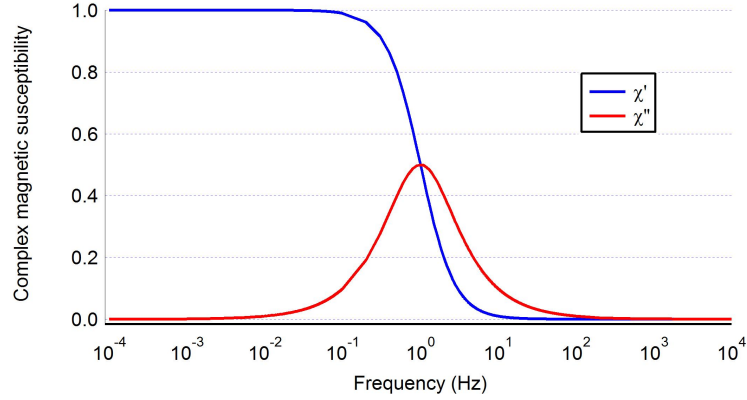


Figure 1–3: Dynamic response of some ferrofluids magnetization considering the Debye model for dipolar systems

mechanisms, the Brownian and Néel relaxations. Brownian relaxation mechanism describes the behavior of the nanoparticle rotation in the direction of the applied magnetic field. Néel relaxation mechanism describes the movement of the magnetic dipole moment in the direction of the applied magnetic flux lines. Both mechanisms can occur in parallel.

An example of a Brownian relaxation time application is using the complex magnetic susceptibility equation in ferrofluids expressing a purely Brownian relaxation mechanism, as is for some cobalt ferrite ferrofluids, in which the hydrodynamic volume can be determined, if the temperature and carrier fluid viscosity are known.[33] There exist other methods to determine such values in addition to the magnetization method previously described. For example, the hydrodynamic radius can be obtained from Dynamic Light Scattering (DLS) measurements, and comparing it with the one obtained from the magnetization method, a close value can be observed [34]. In the same way, the viscosity of a liquid is obtained from complex magnetic susceptibility, and finally compared with theoretical data or experimental values from standard processes. This was a procedure presented by Calero [35], in which a new concept of "nanoscale viscosity" was introduced and investigated. The results of viscosity values obtained from complex magnetic susceptibility are pretty

accurate to the one measured with a rheometer. The complex magnetic susceptibility was obtained using the Quantum Design MPMS XL-7 SQUID Magnetometer, which has a limited frequency range up to 1kHz. The minimum viscosity values to be calculated in a Quantum Design MPMS XL-7 SQUID Magnetometer for a popular particle size of 20nm at room temperature is 51.2cP, which is a high value in comparison with some other common liquid at the same temperature, such as water 1cP and hexane 0.33, for whose "nanoscale viscosity" has not been calculated.

In the case of ferrofluids with a predominant Néel relaxation mechanism, the complex magnetic susceptibility curve have the same behavior as for Brownian relaxation mechanism (Figure 1-3), but appears commonly at higher frequencies. Sometimes, investigations about the Néel relaxation mechanism are preferred over the Brownian relaxation mechanism due to its independence on materials movement or rotation, which allows examination of other nanoparticles parameters, as for example, materials anisotropy. Another example is, in investigations of magnetic fluid hyperthermia, it has been demonstrated that for magnetite nanoparticles synthesized by coprecipitation, both relaxation mechanisms contribute to heat dissipation [36]. In order to obtain a good approximation of power dissipation using the complex magnetic susceptibility, the contribution of Néel relaxation time must be investigated. In order to investigate complex magnetic susceptibility due to the Néel relaxation mechanism, a instrument that measures the complex magnetic susceptibility at high frequencies must be used.

From previous perspectives, an instrument to measure the complex magnetic susceptibility, such as the AC susceptometer, must be developed and improved in its frequency range to allow measurements such as the viscosity of low viscous solvents using the Brownian relaxation equation, or to obtain results of a ferrofluid expressing the complex magnetic susceptibility for a Néel relaxation time. In this work, an AC susceptometer was developed for a frequency range from 10kHz to 1MHz with a

constant excitation field, in which the magnetization of a sample of cobalt ferrite ferrofluid is sensed and used to validate the instrument by comparing the solvent viscosity obtained by means of the complex magnetic susceptibility and the viscosity obtained from theoretical models.

1.3 Motivation

For the purpose of determining fluid viscosity by means of the complex magnetic susceptibility, an expansion of AC susceptometer frequency range at constant magnetic field is designed. This design is expected to open opportunities in prove experimentally the ferrofluid magnetization theory, such as the Debye model in a high frequency magnetic field with constant intensity, and the relationship between nanoparticles complex magnetic susceptibility and power dissipation.

1.4 Objectives

The objective of this thesis was to design and develop a custom-made AC susceptometer to obtain the complex magnetic susceptibility curves of ferrofluids samples. In order to obtain good complex magnetic susceptibility curves, ferrofluids were synthesized considering the frequency range of the system and its magnetization sensitivity. The viscosities were obtained mathematically from the Brownian relaxation time and are compared with viscosity values obtained from literature or validated systems, proving the system functionality. The specific objectives in this work were:

- Design an appropriate AC susceptometer
 - Develop a configuration from which can be maintained a fixed magnetic field intensity in the frequency range of 10kHz-100kHz
- AC susceptometer validation through comparison of theoretical viscosity values with the ones obtained experimentally from the complex magnetic susceptibility

- Suspend cobalt ferrite nanoparticles in different solvents with viscosities suitable to obtain a theoretical loss peak in the frequency range of the AC susceptometer
- Measurement of viscosity by means of complex magnetic susceptibility of nanoparticles suspended in different concentration of mineral oil with hexane.
- Compare the results of viscosity obtained from complex magnetic susceptibility with values found in the literature or measured in the laboratory with a validated system such as the capillary viscometer.

1.5 Outline

The chapters of this document are organized as follows:

Chapter 1 presents a brief introduction and explanation of the AC susceptometer designs. Also, a brief description about ferrofluids and how are used to validate the AC susceptometer is presented. Several reasons to investigate ferrofluids through complex magnetic susceptibility using a wideband AC susceptometer with constant magnetic field intensity are mentioned. Finally, the main motivation and the objectives of this work are presented. Chapter 2 presents the most important theory of electromagnetism and ferrofluids used in this work. Chapter 3 describes the development of an AC susceptometer, and briefly, describes the suspensions of cobalt ferrite nanoparticles in different concentrations of mineral oil and hexane. Chapter 4 shows the result of the measurement of complex magnetic susceptibility for four different ferrofluid, whose solvents are mixtures of 25%w/w hexane-75%w/w mineral oil, 50%w/w hexane-50%w/w mineral oil, 75%w/w hexane-25%w/w mineral oil, 100%w/w hexane. The characterization of the nanoparticles sizes and magnetization are presented. The viscosities obtained from the complex magnetic susceptibility and from a capillary viscometer are compared in order to validate a good instrument functionality. Viscosities comparison was discussed. Finally, Chapter

5 presents the conclusion of the research, in where a 10kHz-1MHz AC magnetic susceptometer with constant excitation field was developed. Good agreement was found between the experimental viscosity and those predicted theoretically from the hydrodynamic diameter of the nanoparticles. Recommendations for AC magnetic susceptometer improvement are mentioned.

CHAPTER 2

THEORETICAL BACKGROUND

This chapter presents an introduction to fundamental theory related to the disciplines applied to this work, electromagnetism and fluid mechanics. The information of electromagnetism presented focuses on basic theory used to derive mathematical models that describes the generation and behavior of a magnetic fields, and explain the response of a material to an applied magnetic field. The second theoretical information presented is about fluid mechanics, in where its principles used to obtain equations that describes the dynamics of a fluid and its interaction with solid matter, leads to the main theory of ferrofluid magnetic properties.

2.1 Electromagnetism

2.1.1 Relationship between magnetic field and current

Electromagnetism is responsible for interactions between charged particles [2]. Consequences of these forces are electricity and magnetism. Electricity is the phenomenon describing the presence of a charge, its electric field and the effect on another charge. On the other hand, magnetism is the physical phenomena of a material at atomic or subatomic level exerting or responding to an attractive or repulsive magnetic field forces, which is commonly associated with the motion of electric charges.

An important term related to electricity is the voltage, which has a direct relationship with electric fields, and is further related with the concepts of magnetism.

Voltage is the difference of potential existing in an electric field. This is given by

$$V = - \int \mathbf{E} \cdot d\mathbf{l} \quad (2.1)$$

where \mathbf{E} is the electric field in newtons/coulomb (N/C) or volts/meter (V/m). When a connection, usually a conductive material, with a resistance R is applied between these two potentials, a flow of charges will exist, leading to the appearance of current I . This was explained by Ohm, whose law is given by

$$V = IR \quad (2.2)$$

where I is the current in ampere (A), opposite to the flow of negative charges, and R is the resistance in ohms (Ω) which opposes the flow of charges. In addition to the electric field due to the presence of charges, there will be a magnetic field due to the movement of these charges. This is given by Biot-Savart's law

$$dH = \frac{I dl \sin \phi}{4\pi r^2}. \quad (2.3)$$

Biot-Savart's law states that the differential of the magnetic field intensity H in ampere/meter (A/m) produced by a differential current element is proportional to the product of the differential current element and the sine of the angle between the element and the line joining P to the element and is inversely proportional to the square of the distance between the point of measurement and the current element [2].

A simplified form of the Biot-Savart equation used for the generation of a magnetic field by a number N of current loops is given by,

$$\mathbf{H} = \frac{NI}{l} \quad (2.4)$$

in which l is the length of the coil. Equation 2.4 is also known as the magnetic field for infinite coil approximation.

An analysis in the opposite direction could be performed, in where a current is created from a magnetic flux. Faraday discovered that the induced electromotive force (emf), V_{emf} (in volts), in any closed circuit is equal to the time rate of change of the magnetic flux linkage by the circuit [2]. This is established by

$$V_{emf} = -N \frac{d\Psi}{dt} \quad (2.5)$$

where the negative sign the the Lenz's law, which describes the effect of the currents generating a magnetic field which opposes to the original change of magnetic flux. The magnetic flux describes the behavior of the magnetic field through any surface material. The magnetic flux equation is given by

$$\Psi = \int_S \mathbf{B} \cdot d\mathbf{S} = BA \quad (2.6)$$

in which A is the area perpendicular to the magnetic flux lines, and B is the magnetic flux density, which depends on the material properties. Following sections introduce concepts about the behavior of materials under the presence of a magnetic field.

2.1.2 Magnetic force and magnetic dipole moment

A magnetic force is exerted on moving electrically charged particles in a magnetic field [37]. This is called the Lorentz force, and is given by

$$\mathbf{F} = q(\mathbf{E} + \mathbf{v} \times \mathbf{B}) \quad (2.7)$$

This is the net force exerted on a charge if the charge moves through a region of space in which there are both an electric field and a magnetic field [38]. In terms of the atomic scale, the orbiting electrons and the spins contribute to the generation of atomic currents. Considering an atomic current loop as in Figure 2-1, which has a small magnitude of current I and a loop surface area S , a magnetic dipole moment

appears in the direction perpendicular to the loop and is given by

$$\mathbf{m} = IS\mathbf{a}_s \quad (2.8)$$

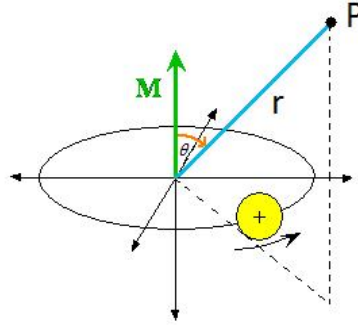


Figure 2–1: Magnetic moment generated by a positively charged particle. A magnetic field at point P is generated by the current loop

The magnetic flux density at a point P due to the atomic current loop is given by

$$\mathbf{B} = \frac{\mu_0 m}{4\pi r^3} (2 \cos \theta \mathbf{a}_r + \sin \theta \mathbf{a}_\theta) \quad (2.9)$$

At the atomic scale, previous concepts can be similarly applied to any independent charge in movement. Similar concepts and equations could be used in complex structures, as for magnetic materials, in which subdivisions of the material possess different properties, and act different under an applied magnetic force.

2.1.3 Magnetic materials

The magnetic phenomena presented previously could affect some materials, in such a way that they could suffer deformations, alterations of their internal magnetic properties, or physical position changes. Magnetic susceptibility and permeability are two important terms that describe how much effect a magnetic field has in a material. Magnetic susceptibility χ , which is unitless, parameterizes how easy it is for a material to respond to a magnetic field. The permeability (μ), with dimensions henries per meter (H/m), is a property specific to the material through which H field passes and in which B is measured. The magnetic susceptibility and the relative

permeability are related as follows

$$\chi = \frac{\mu}{\mu_0} - 1 \quad (2.10)$$

where μ is the permeability of the material and μ_0 is the permeability of the vacuum. The magnetic field strength and flux density are related according to

$$B = \mu H \quad (2.11)$$

In the presence of a H field, the magnetic moments within a material tend to become aligned with the magnetic field and to reinforce it by virtue of their magnetic field [37]. This corresponds to

$$B = \mu_0(H + M) \quad (2.12)$$

where M is the magnetization of the solid. Substituting Equation 2.10 in Equation 2.12 leads to

$$M = \chi H \quad (2.13)$$

The magnetic moment can be considered to be a vector quantity with a direction determined by the materials structure, which could be a monocrystalline structure or a polycrystalline structure. Figure 2-2 presents an example of a monocrystalline and polycrystalline material,

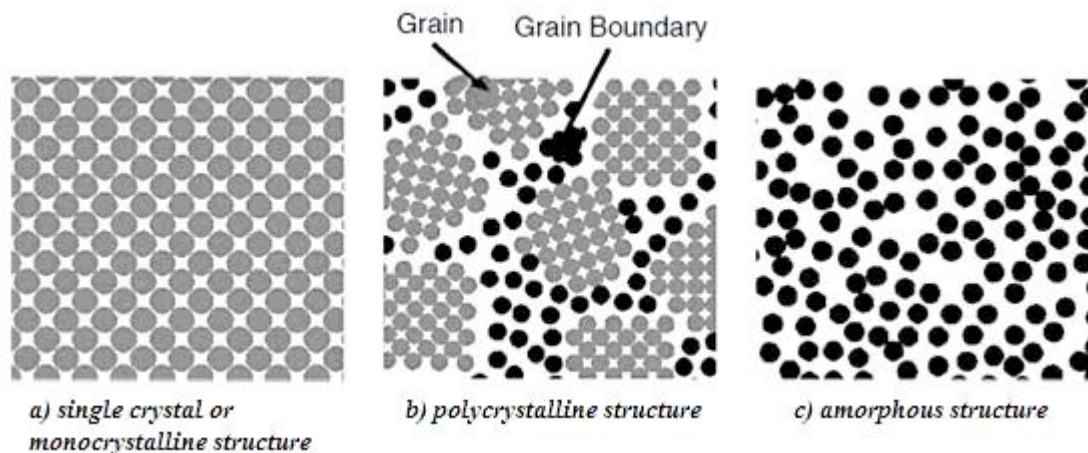


Figure 2-2: Schematic of single crystal or monocrystalline, polycrystalline, and amorphous material structures [39]

A monocrystalline material, also called single crystal material, is defined as a material with a periodic arrangement of atoms extended through all its structure [37], implying that the same properties can be observed across the material if all the structure is under the same applied conditions, such as temperature and stress, among others. In the case of polycrystalline materials, the structure is composed of many different smaller crystals or grains. These grains are divided by some atomic mismatch that exists within the region where two grains meet, which is called the grain boundary. Noncrystalline materials, also called amorphous materials, lack of a systematic and regular arrangement of atoms in where atomic distances are relatively large. Each single crystal possesses physical properties, such as electrical conductivity, elastic modulus, and others, could depend or not on the crystallographic direction. Materials whose measured properties are independent of the direction of measurement are called isotropic. Some materials have variations of atomic or ionic spacing, driving the properties to depend on directions. The materials whose properties depend on crystallographic directions are called anisotropic [37]. Anisotropic materials do not behave the same way in all directions. Figure 2-3 illustrates the mechanical behavior of isotropic and anisotropic materials.

Different kinds of atomic configurations in materials allows the existence or vacancy of dipoles, leading to the formation of a variety of magnetisms, such as diamagnetism, paramagnetism, ferromagnetism and ferrimagnetism.

Diamagnetism is a very weak form of magnetism that is non permanent and persists only while an external field is being applied. It is induced by a change in the orbital motion of electrons due to an applied magnetic field [37]. In this case, the orbital motion generates a field opposite to the applied field (magnetization is directed oppositely to the field, as illustrated in Figure 2-4). Diamagnetism is found in all materials; but because it is so weak, it can be observed only when other types of magnetism are totally absent [37].

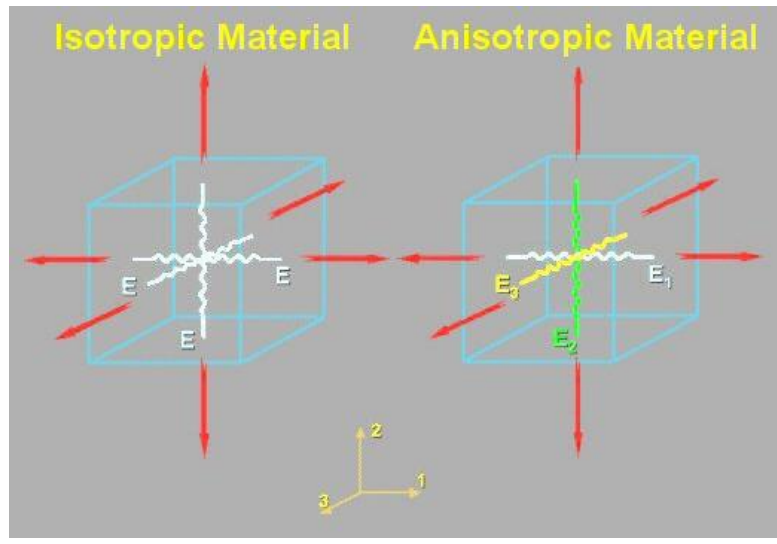


Figure 2-3: Behaviour of isotropic and anisotropic materials, in where variable E represents the Young Modulus. This figure shows that the stress in response to a strain varies with direction[40]

Paramagnetism results when in a material, the magnetic moments preferentially align, by rotation, with an external magnetic field as shown in Figure 2-5. This material possesses no net macroscopic magnetization because the orientation of these atomic magnetic moments is random in the absence of an external magnetic field.

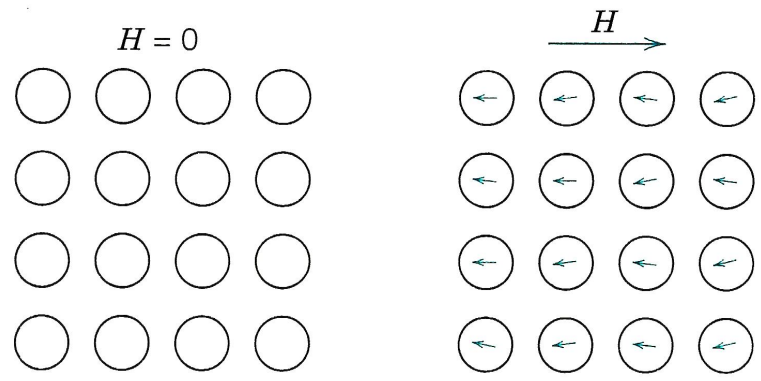


Figure 2-4: Atomic dipole configuration for a diamagnetic material [37]

Figure 2-6 presents the magnetization curves for diamagnetic and paramagnetic materials.

Ferromagnetism arises from the permanent magnetization of the magnetic moments in the absence of the magnetic field. Permanent magnetic moments in ferromagnetic materials results from atomic magnetic moments due to electron spins

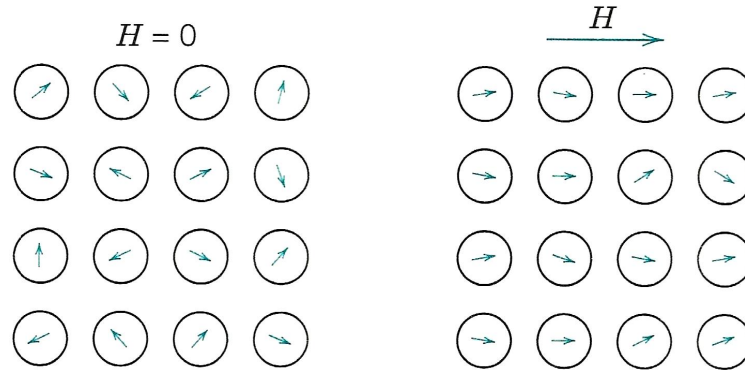


Figure 2-5: Atomic dipole configuration for a paramagnetic material [37]

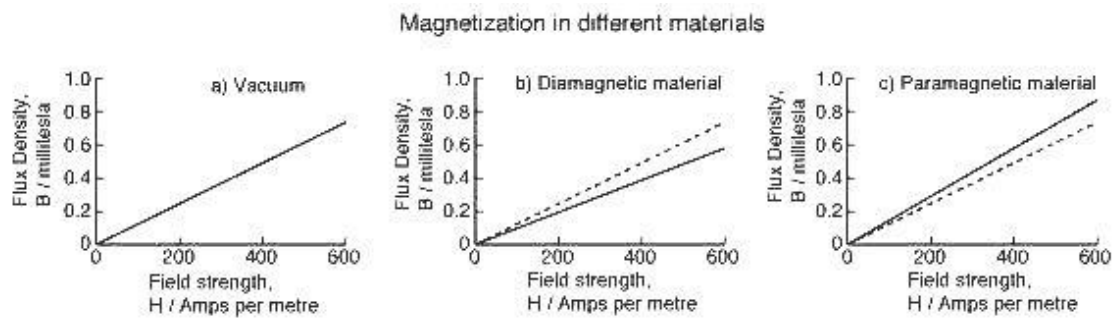


Figure 2-6: Magnetization curves of vacuum, diamagnetic and paramagnetic material [41]

as a consequence of the electron structure. There is also an orbital magnetic moment contribution that is small in comparison to the spin moment. Additionally, coupling interactions cause net spin magnetic moments of adjacent atoms to align with one another, even in the absence of an external field. For this reason, when a ferromagnetic material is magnetized in one direction, the magnetization relaxation will not achieve to zero when the magnetizing field is removed. This residual of magnetization is called the remanence. An opposite magnetic field can drive the magnetization back to zero. The magnetic field force applied to drive the magnetization to zero is called the coercivity. When an AC magnetic field is applied to the material, its magnetization traces a loop called a hysteresis [42]. Figure 2.7 presents the hysteresis curve for a ferromagnetic material.

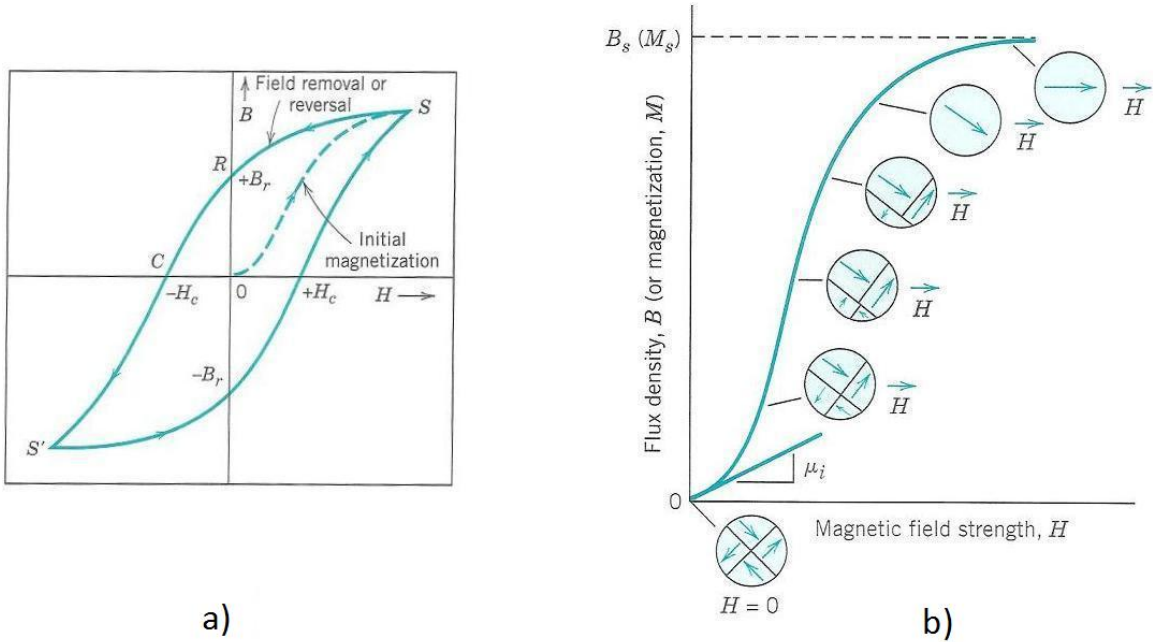


Figure 2–7: a) Typical hysteresis magnetization curves, with a saturation S , a remanence R and a coercive form H_c . b) Magnetic flux density (B) versus magnetic field intensity (H) behavior for ferromagnetic and ferrimagnetic materials, in where is presented the material with initial permeability μ_i , and whose domain adopt different configurations during several stages of magnetization until it reaches saturation.[37]

Ferrimagnetism is a permanent magnetization presented by ceramics, with macroscopic magnetic characteristics similar to those from ferromagnets. The net ferromagnetic moment arises from the incomplete cancelation of spin moments. The macroscopic magnetic characteristics of ferromagnets and ferrimagnets are similar; the distinction lies in the source of the net magnetic moment [37]. Although ferromagnetic and ferrimagnetic materials have different magnetic ordering, ferrimagnetic materials exhibit all the hallmarks of a ferromagnetic material behavior such as permanent magnetization, hysteresis, and remanence [43].

Another two different types of magnetism, antiferromagnetism and superparamagnetism, are recently studied due to their existence in uncommon materials. In antiferromagnetism, adjacent dipoles spontaneously align in an antiparallel arrangement, presenting no gross external magnetic field. This spontaneous antiparallel coupling, observed in solids such as manganese oxide (MnO), appears by heating

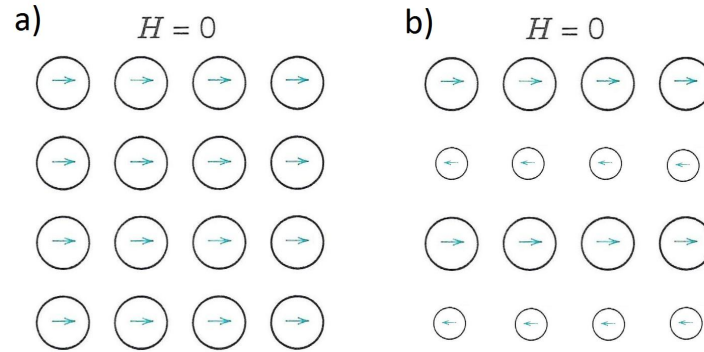


Figure 2–8: Ordering of the atomic dipoles in a) ferromagnetic and b) ferrimagnetic material [37]

the material and disappears entirely above the Néel temperature, which is characteristic of each antiferromagnetic material.[30] Finally, superparamagnetism is a form of magnetism usually found in very small ferromagnetic and ferrimagnetic nanoparticles ($\sim 100 - 10$ angstroms (Å)). There are two main reasons that allow these ferromagnetic and ferrimagnetic nanoparticles to exhibit superparamagnetism: anisotropy and size. For example, for small nanoparticles with a predominant Néel relaxation time and a active magnetic core between 2-3nm, their magnetization appears to be an average of zero when the time used to measure the magnetization is longer than the Néel relaxation time. In this case, the nanoparticles are in the superparamagnetic state.

In order to understand how nanoparticles interacting with a fluid behaves to an applied magnetic field, next section presents a brief introduction to fluid mechanics, which is emphasize in the equations that are related to the ones of interest, such as the equations of viscosity and nanoparticles magnetization.

2.2 Fluid Mechanics

2.2.1 Fluid Properties

Fluid mechanics is the branch of the physical sciences concerned with how fluids behave at rest or in motion [44]. Fluid mechanics can be divided into fluid kinematics, the study of fluid motion, and fluid dynamics, the study of the effect of forces on fluid motion, which can further be divided into fluid statics, the study of

fluids at rest, and fluid kinetics, the study of fluids in motion. The branch of fluid mechanics which study the materials with both, solid and fluid characteristics, is called rheology. Rheology is also defined the science of the deformation and flow of matter [45].

The first main goal of rheology consist of establishing the relationship between applied forces and geometrical effects induced by forces at a point [46]. The mathematical form of this relationship is called the rheological equation of state, which is a thermodynamic equation describing the state of matter under a given set of physical conditions. The Newton and Hooke laws are the simplest examples of such equations.

Newton reflected upon a resistance of liquids to a cylinder rotating in a vessel. According to this, the deformation rate is expected to be proportional to stress and the constant coefficient of proportionality is called viscosity, which is a material parameter of liquid. Newton's law for the common case of incompressible liquids, also called Newtonian liquid, is given by

$$\dot{\gamma} = \frac{\tau_s}{\eta} \quad (2.14)$$

where $\dot{\gamma}$ is the rate of shear deformation, or also the velocity gradient in velocity units [m/s]. τ_s is the shear stress in Pascals [Pa], and η is the viscosity, or more specifically, the dynamic viscosity, in Pascal seconds [Pa·s], or Poisse [P] units. This law assumes that, in flow of liquids, a force, commonly the resistance to flow, is proportional to a velocity.

Hooke formulated a similar proposal concerning properties of solids. This law was translated by Bernoulli and then by Euler. Hooke's law states that in deformation of solids, stress is proportional to deformation, which is given by

$$\varepsilon = \frac{\sigma_Y}{Y} \quad (2.15)$$

The coefficient of proportionality Y is the elastic modulus, also called Young's modulus, which have units of pressure. The tensile stress is written by σ_Y in pressure units, and the deformation or strain is ε which is dimensionless.

Rheological equations of state are used to describe many materials, even though these can be very different for numerous real materials. However, there are many other materials which are not described by previous equations. Rheology relies on the concept that *non-Newtonian* and *non-Hookean* materials exist in reality. Fluids which present a non-Newtonian behavior exhibit a shear stress which is not proportional to the shear strain rate.[46] A graph of this behavior for Newtonian and non-Newtonian fluids is presented in Figure 2-9.

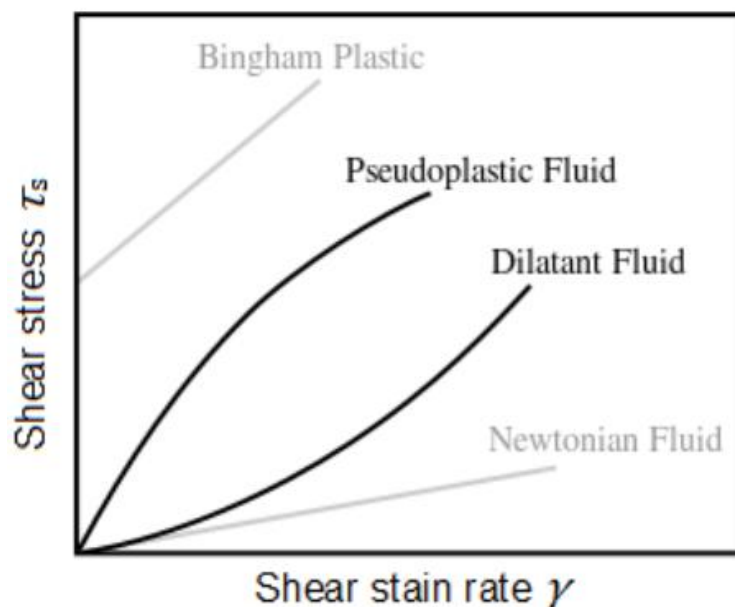


Figure 2–9: Comparison of the shear stress vs shear rate behavior in one Newtonian fluid, such as water, and two non-Newtonian fluids, such as the dilatants and the pseudoplastic fluids. Dilatants increase in apparent viscosity at higher shear rates, different from pseudoplastic fluids that have a lower apparent viscosity at higher shear rates. An example of dilatants and pseudoplastic fluids are printing inks and starch solution, respectively.[47] Another non-Newtonian material not strictly a liquid is the Bingham plastic, which is a viscoplastic material that behaves as a rigid body at low stresses but flows as a viscous fluid at high stress.[48]

Colloidal suspensions are an example of a non-Newtonian fluid. Non-Newtonian flow is found only in colloidal and other particulate system (in which the concept

of colloidal particles includes large molecules). Suspensions of rigid, non-interacting spheres in a Newtonian liquid should exhibit Newtonian flow. The nonlinear flow curves observed from colloidal and other dispersed systems can be explained by interactions between particles, interactions with the continuous phase, and particle deformation.[45]

The Bernoulli effect, whose principle states that an increase in the speed of the fluid occurs simultaneously with a decrease in pressure or a decrease in the fluid's potential energy, as well as van der Waals' attraction, causes particles to come together. This attraction may be reinforced by the presence of positive and negative electrostatic charges and hydrogen bonding. On the other hand, high surface charges of like sign cause interparticle repulsion. Spongelike particles at macro- and microscopic scale can immobilize large amounts of the surrounding liquid.[45] Liquid mobility can be lowered by the nanoparticles interaction with the solvent, which creates a hydrodynamic layer on the nanoparticles. This is the effect occurring in ferrofluids. Particles can be suspended in a Newtonian fluid, however, the particles in a fluid as a whole system commonly exhibit a non-Newtonian behavior.

2.2.2 Magnetic fluids

Viscosity

Previous rheological equations of state found for different materials are used to solve macroscopic problems related to continuum mechanics of these materials. A different approach of rheology consists of establishing relationships between rheological properties of materials and its molecular structure (composition). This is an independent second goal for rheology, which is related to estimating quality of materials, understanding laws of molecular movements and intermolecular interactions.[46]

The standard method to determine viscosity of a fluid is a capillary viscometer, which determine the kinematic viscosity in Stokes units [St]. The dynamic viscosity,

in Poise units [P], is derived from the product of the kinematic viscosity and the fluid's density. Usually, the fluids measured in a common capillary viscometer are Newtonian because most capillary viscometers measure viscosity at one shear rate at a time [49]. A more common instrument used to determine viscosity of non-Newtonian fluids is the rheometer. A very important application of rheometers is the measurement of ferrofluids viscosity, in which could be determined the behavior of the ferrofluid viscosity under an applied magnetic field.

The viscosity of a ferromagnetic suspension is greater than that of carrier fluid and accompanies an increased rate of energy dissipation during viscous flow due to presence of the suspended particles. This is the same situation in mixtures of non-magnetic particles suspended in a liquid. A classical equation is presented by Einstein relates the mixture viscosity η to the carrier fluid viscosity η_0 and solids fraction (assuming particles bare of coating):

$$\eta/\eta_0 = 1 + \frac{5}{2}\phi_v \quad (2.16)$$

This relationship applies for small concentrations. An equation for higher concentrations presented by Rosensweig, Nestor, and Timmins, assume a two-constant expression:

$$\eta/\eta_0 = 1/(1 + a\phi_v + b\phi_v^2) \quad (2.17)$$

Equation 2.17 reduces to equation 2.16 for small values of ϕ_v so that $a = -\frac{5}{2}$. At a concentration ϕ_c the suspension becomes effectively rigid, and η_0/η goes to zero. Thus the second constant is $b = (\frac{5}{2}\phi_c - 1)/(\phi_c^2)$. $\phi_v = 0.74$ is the value that corresponds to close packing of spheres. An uncoated spherical particles of radius r , existing in a ferrofluid with volume fraction ϕ_v , will occupy a fractional volume in the fluid of $\phi_v(1 + \delta/r)^3$ when coated with a uniform layer of dispersing agent having thickness δ . A combination of these equations gives

$$\frac{\eta - \eta_0}{\phi_v \eta} = \frac{5}{2} \left(1 + \frac{\delta}{r_p}\right)^3 - \left(\frac{\frac{5}{2}\phi_c - 1}{\phi_c^2}\right) \left(1 + \frac{\delta}{r_p}\right)^6 \phi_v \quad (2.18)$$

When a magnetic field is applied to a magnetic fluid subjected to shear deformation, the magnetic particles tend to remain rigidly aligned in the orientation of the magnetic flux lines. An important effect observed is that when the fluid vorticity and the magnetic field are parallel, the particles can rotate freely and magnetism exerts no influence on the viscosity, given by Einstein relationship. When the directions are perpendicular, the magnetic contribution to the viscosity is maximized.

Magnetic Properties

The magnetic and physical properties of a ferrofluid such as its equilibrium magnetization in steady applied field, magnetization change in a field of shifting orientation or intensity, or shear stress versus rate of strain, are important for the proper formulation and interpretation of the ferrohydrodynamic description of the fluids.

The particles in a ferrofluid, each with its embedded magnetic moment m , are analogous to the molecules of a paramagnetic gas or material. As previously mentioned, when no field exists, the particles are randomly oriented, and the fluid has no net magnetization. However, in the presence of an ordinary field, the tendency of the dipole to align with the applied field is partially overcome by thermal agitation. As the magnitude of the magnetic fields is increased, the particles become more aligned with the field direction, until these are almost completely aligned. At this point, the magnetization achieves its saturation value. Further, Langevin's classical theory is adapted to an apparent superparamagnetic behavior leaded by the two relaxation mechanisms, in which is assumed that there is negligible particle-particle magnetic interaction [50].

The magnitude of the torque applied on the particles by the presence of the magnetic field is given by

$$\tau_q = mH \sin \theta \quad (2.19)$$

where H is the magnetic field intensity and θ is the angle between H and the domain magnetization M_d , which is intrinsic in the magnetic moment m . This moment equals $\mu_0 M_d V$ where V is the volume of the particle. The magnetization M of a ferrofluid has the direction of the applied field and its magnitude is the total of moments of the magnetic particles suspended in a unit volume of the mixture [50],

$$\mu_0 M = n\bar{m} \quad (2.20)$$

where \bar{m} is the component of the mean magnetic moment per particle along the field direction. When the field is reduced from saturation, the magnetization curve closely retraces its original path. For this reason, a small area of the hysteresis loop is observed, and values of remanence and coercivity field are almost zero.

The Debye model describes the dynamic response of the magnetization. Assuming monodisperse particles, the magnetization of the particles is described by

$$M = \chi' H_0 \cos(\Omega t) + \chi'' H_0 \sin(\Omega t) \quad (2.21)$$

where Ω is the angular frequency, χ' is the in-phase and χ'' the out-of-phase component of the dynamic susceptibility, which are frequency dependent. For an effective magnetic relaxation time constant τ , both components are given by

$$\chi' = \frac{\chi_0}{1 + \Omega^2 \tau^2} \quad (2.22)$$

and

$$\chi'' = \frac{\chi_0 \Omega \tau}{1 + \Omega^2 \tau^2} \quad (2.23)$$

There are two mechanisms that describe the relaxation of the nanoparticle magnetization after the applied field has been changed. The first mechanism, the

Brownian rotational diffusion time τ_B , emphasized the particle rotation mechanism. This is given by

$$\tau_B = \frac{3V_H\eta_0}{kT} \quad (2.24)$$

where V_H is the particle volume and η_0 the dynamic viscosity of the carrier fluid. The magnetization of a single-domain uniaxial ferromagnetic particle when no field exists has two possible orientations, the opposite directions along the easy axis of magnetization. An energy barrier must be overcome to move from one orientation to the other and is given by KV , where K is the magnetic anisotropy constant of the material. When $KV \ll kT$, the thermal energy is large enough to induce fluctuations of the magnetization inside the grain with a characteristic time τ_N . This was obtained by Néel and given as

$$\tau_N = \frac{1}{f_0} e^{\frac{KV_H}{kT}} \quad (2.25)$$

where f_0 is a frequency with approximate value of 10^9 Hz. The prevailing mechanism is determined by the one having the shortest relaxation time. Both mechanisms lead to an apparent superparamagnetic behavior, which is described by Langevin's law, whose relationship describes the equilibrium response [50]. The effective magnetic relaxation time constant is given by

$$\tau = \frac{\tau_N\tau_B}{\tau_N + \tau_B} \quad (2.26)$$

Composition

The properties of ferrofluids, are profoundly affected by the thermal Brownian motion of the suspended particles and the circumstance that each subdomain particle is permanently magnetized. Also, some of the rheological properties, such as viscosity, are affected. These properties depend also on their chemical preparation.

Therefore, in addition to the particles and the carrier liquid, the presence of an adsorbed long-chain molecular species on the particle surface is an essential ingredient that prevents agglomeration of the particles.

There are two conventional methods of preparing a ferrofluid, preparation by size reduction and by precipitation that is, making little particles out of big ones and producing little ones from solution initially. In current work, another method known as thermo-decomposition is used to synthesize the nanoparticles. Cobalt and iron, both with their corresponding oleate are exposed to this process to obtain the cobalt ferrite $CoFe_2O_4$ in oleic acid. Further, the $CoFe_2O_4$ is diluted in different fluids like mineral oil, hexane and octadecene. In addition, mixtures of various proportions are created in order to obtain different viscosities and observe CMS curves behavior to compare them.

CHAPTER 3

EXPERIMENTAL PROCEDURE

This chapter presents the design of the AC susceptometer in detail. The features allowing an increase of the frequency range up to 1MHz such as the development of a very high speed instrumentation amplifier and the design of low inductive/low capacitive coils are explained. This section also presents the synthesis, suspension and characterization of the cobalt ferrite ferrofluids used to validate the AC susceptometer by determining viscosity of its carrier fluid, and comparing it with theoretical and validated values.

3.1 AC susceptometer design

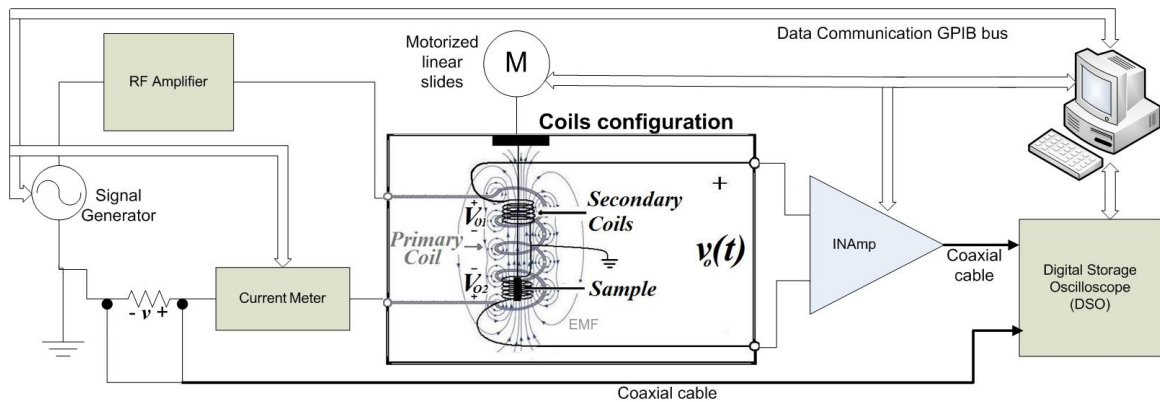


Figure 3–1: Diagram of the AC susceptometer configuration. The input sinusoidal signal is amplified to enhance the magnetic field which decreases at higher frequencies due to the inductive impedance of the primary. A first order gradiometer as secondary coil senses the magnetization of the sample due to the applied AC magnetic field. The differential signal detected by the INamp is compared with the current source signal, measured from the resistor voltage, for phase-shifts and amplitude variations.

Figure 3-1 shows the AC susceptometer configuration. The input sinusoidal signal is amplified to enhance the magnetic field which decreases at higher frequencies due to the inductive impedance of the primary. A first order gradiometer as secondary coil senses the magnetization of the sample due to the applied AC magnetic field. The differential signal detected by the INAmp is given by,

$$v_0(t) = \frac{\mu_0 \omega |\chi| N_1 N_2 A_2 I_1}{l} e^{j(\omega t + (\theta_I + \theta_\chi + 90^\circ))} = V_0 e^{j(\omega t + \theta_{v0})} \quad (3.1)$$

where ω is the angular frequency of the magnetic field, μ_0 is the vacuum permeability, χ is the magnetic susceptibility, I is the current, V_0 is the output voltage magnitude, θ_v is equal to $\theta_I + \theta_\chi + 90^\circ$, in where θ_I is the phase of the current through the primary and θ_χ is the phase difference between the vectors of the magnetic field intensity and the magnetization, l is the coil length, and N_1 and N_2 are the number of turns of the primary and secondary, respectively. This mathematical model assumes that just one frequency component is induced in the secondary. The measured differential voltage is compared with the current source signal, obtained from the resistor voltage, for phase-shifts and amplitude variations caused by the sample. The magnitude and phase of the output voltage is calculated from the in-phase and the out-of-phase components. The in-phase component is the amplitude of the secondary signal when the primary signal is 0° , and the out-of-phase component corresponds to the amplitude of the secondary signal when the primary signal is 90° . If any imperfection exists in the construction of the secondary arrangement, there will be an imbalance signal. This imbalance can be canceled by measuring the difference of the output voltage when the sample is inside the upper and the lower pickup coils. The corrected output voltage is given by

$$V_0 = \frac{V_{01} - V_{02}}{2} \quad (3.2)$$

Equation 3.1 can be used to obtain the real and imaginary part of the magnetic susceptibility,

$$|\chi| = \frac{V_0 l}{\mu_0 N_1 N_2 \omega A I} \quad (3.3)$$

$$\theta_\chi = \theta_{v0} - \theta_I - 90^\circ \quad (3.4)$$

In this way, a complex magnetic susceptibility versus frequency curve can be obtained and used to determine the nanoparticle relaxation time from the χ'' peak. The AC susceptometer configuration used in this work has additional design features which allow a range of up to 1MHz.

3.1.1 System Development

Coil assembly. The secondary is a symmetric first-order gradiometer. For both the primary and secondary coils, Carol A 18 AWG (American Wire Gauge) wire was used. The thickness of this cable is sufficient to avoid a considerable effect of the parasitic capacitances between each turn of wire in the proposed frequency range. The primary and the secondary have just one layer with 82 turns and 7 turns, respectively. The wires going out of the coils back to the RF Amplifier and to the INamp are twisted pair. A 22 AWG wire is used to ground the center point between the two coils of the secondary. Figure 3-2 shows a picture of the actual assembly.

Sample Holder. The sample holder is a cylinder made of a non-magnetic polycarbonate with a diameter of 8mm and a length of 20mm. This dimension is very close to that required to fill the internal volume of the pickup coil and obtain a maximum output voltage due to the sample. The same reed of the Quantum Design MPMS is used to carry the sample holder to the AC susceptometer coils.

Electronics. Considerable attention must be given to the sensing bridge due to high frequency effects. In order to have a high signal-to-noise ratio, a high output voltage range must exist in comparison to the imbalance signal and noise floor. Common commercial instrumentation amplifiers lack some features necessary



Figure 3–2: Picture of the coils. A Carol A 18 AWG wire was used for the primary and secondary coils.

to achieve a linear output signal, such as high slew rate. Due to the very high speed and voltage feedback architecture, three LM7171 op-amps were used to develop a very high speed instrumentation amplifier as presented in the LM7171 datasheet. Figure 3-3 illustrates the schematic of the developed instrumentation amplifier.

Although current feedback amplifiers present ideally unlimited slew rate and high full power bandwidth, voltage feedback amplifiers are preferred due to the wide range of resistor values that can be used to set the gain [51] and its matched input impedance, which is suitable for differential configurations [52]. Figure 3-4 shows the actual instrumentation amplifier.

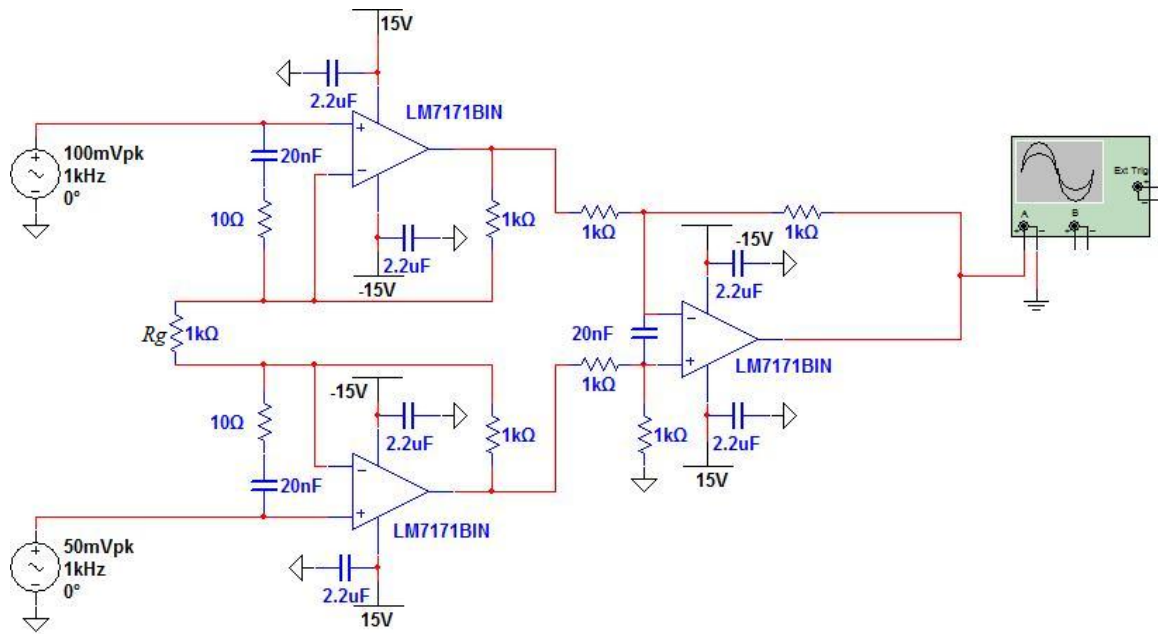


Figure 3–3: Instrumentation amplifier constructed with three LM7171. Input-lag compensation was added to the two op-amps at the input to obtain stability. As well, a capacitor were added to the differential op-amp. For this application adding a resistor to obtain input-lag compensation compromises stability. All resistors have fixed values except R_g which is variable.

Although very good performance is observed in the LM7171 for simple applications such as fixed input voltage, non-inverting and inverting configurations, high input impedances, and small frequency variations, problems with stability are observed in applications requiring more dynamics and complex configurations. To avoid this problem, in each of the input op-amps, an input-lag compensator [53] is added. For the differential stage, the INamp works stably with high impedance source at the input, with or without adding an input-lag compensator. Very low impedance sources at the input of the INamp, as is the secondary coil, arise stability problem whether or not an input-lag compensator is added. By leaving a capacitor between the inverting and non-inverting input of the differential stage, stability is obtained. In addition to, some design considerations of printed circuit board (PCB), such as the use of capacitor to bypass the power supply ripple and high frequency noise, and the reduction of unwanted capacitances in the inverting input

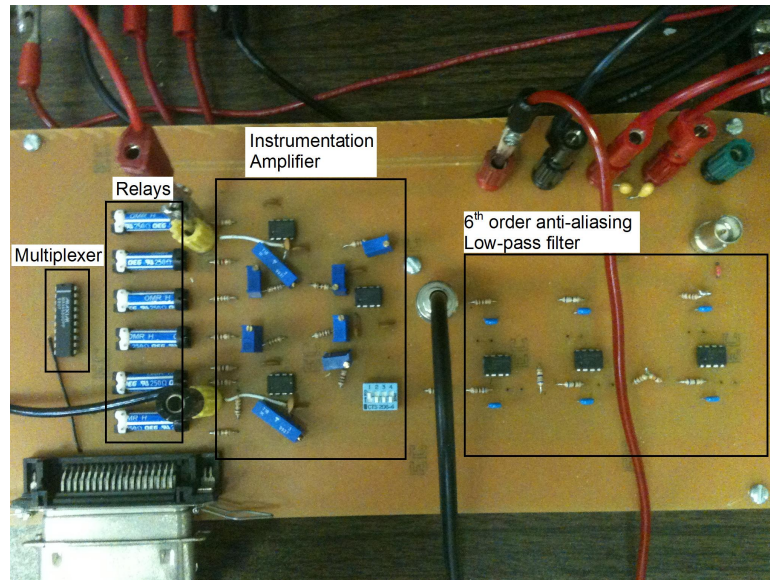


Figure 3–4: Picture of the instrumentation amplifier. Due to the unwanted internal input impedance of the multiplexer, relays are used to change between several gain resistors (R_g), which is the resistor establishing the gain. The relays are controlled with a multiplexer, which is controlled with the computer by parallel port. At the right, an anti-aliasing 6th order low-pass filter, which is currently in progress for future system optimization.

by reducing trace width and placing components close to this input, are crucial in maintaining low noise and avoiding circuit oscillations.[54] A good instrumentation amplifier performance is observed in Figure 3-5, which presents the frequency and phase response. A small overshoot-like signal caused by the capacitor added in the differential stage is observed between 500 kHz and 800 kHz.

AC susceptometer equipment. An Agilent 33120a signal generator is used to generate the sine wave, which is sent to the 1140LA E&I amplifier in order to obtain the necessary voltage to maintain a constant current source. To measure the current across the excitation coil, an Agilent 34401a multimeter is used between the primary and the power resistor. The power resistor is placed at the end because the probe used to measure the voltage in the power resistor has a connection to ground. The primary and secondary signals are observed in an Agilent 54622D oscilloscope. The sample is moved between the two pickup coils with a Zaber Motorized Linear Slide. Figure 3-6 shows a picture of the complete AC susceptometer.

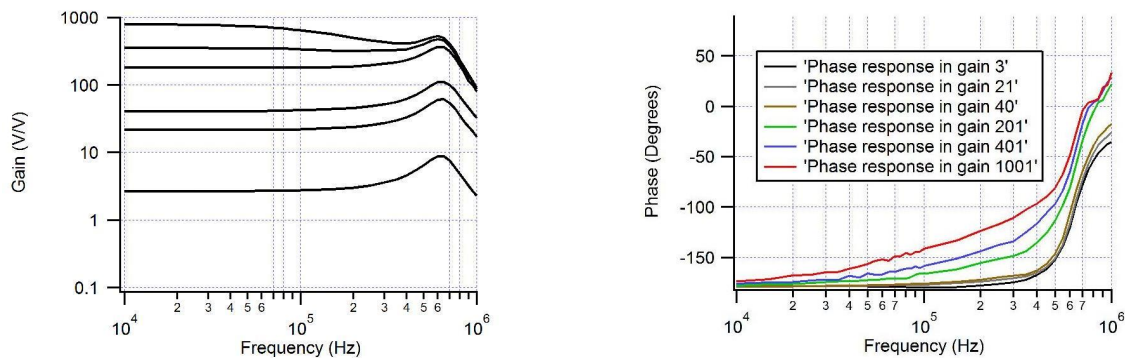


Figure 3–5: Gain vs frequency plot (left) and phase vs frequency plot (right) for the instrumentation amplifier constructed with LM7171. A small overshoot-like signal caused by the capacitor added in the differential stage is observed between 500 kHz and 800 kHz.



Figure 3–6: Complete AC susceptometer equipment at laboratory facility.

Automation. The AC susceptometer is fully automated using a PC with Lab-View software. The multimeter, oscilloscope, and generator are controlled and used to receive data through GPIB. The oscilloscope is programmed to acquire four cycles every frequency step. The generator output signal is monitored to send the appropriate voltage to drive one ampere in the primary, in order to obtain 4.25Oe. A parallel port is used to control the gain in the INamp, and through a serial bus the information is sent to move the Zaber actuator, which positions the sample inside the upper or lower coil of the secondary. During sample measurement, the virtual

instrument (VI) acquires in each frequency and each actuator position a quantity of measurements established by the user, which is currently 100 values of in-phase and out-of-phase. The VI also calculates the mean of the 100 measurements. The mean values are sent to a preprogrammed spreadsheet in where the data is saved. The quantity of measurements acquired in each frequency will depend on the ferrofluid. Higher quantity of measurements to mean provides higher accuracy in the complex magnetic susceptibility results. On the other hand, higher quantity of measurements will require more experimentation time, which must be considered for ferrofluids with high volatile solvents, or when exist possibility of aggregation.

3.1.2 Setup Procedure

The presented AC susceptometer has similar operation to the one designed by Nikolo.[55] The reed is positioned in the Zaber motor in such matter that the sample is positioned in one of the secondary's coils. The pickup coils present an output voltage due to the magnetization of the sample inserted inside one of the secondary coils. The sample optimum position inside the secondary coil is found when the maximum output voltage is obtained, which means a maximum inner coil volume filled by the sample. The pickup signal is then analyzed and compared with the signal of the primary in order to obtain the phase-shifts and amplitude variations across the frequency sweep. From equation 3.3 and 3.4, the complex magnetic susceptibility is obtained.

Calibration. Due to the absence of a complex susceptibility and a constant magnetization across the frequency sweep up to 10 kHz, dysprosium oxide (Dy_2O_3) is used to calibrate the system for phase-shifts and amplitude variations caused by the output bridge, coil imperfections, and any constant external perturbations.[56][57] It is assumed that the (Dy_2O_3) has constant magnetization up to 1MHz.

In order to maximize the magnetization of the dysprosium oxide in the sample holder, the volume is filled and fixed with Dy_2O_3 powder, different from some methods in which the Dy_2O_3 powder is mixed with epoxy to obtain a solid structure. Figure 3-7 shows the calibration curve used for one set of measurements.

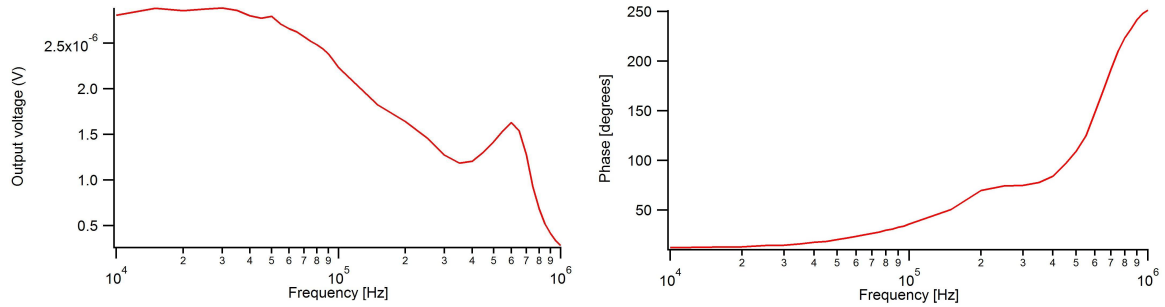


Figure 3–7: Gain and phase AC susceptometer calibration with Dy_2O_3 at maximum instrumentation amplifier gain of approximately $G=800V/V$

Although gain and phase calibration is used to cancel phase-shifts and amplitude variations caused in the instrument, such calibration are not enough to obtain validated magnetization magnitude values due to imperfection in construction which avoids matching of the experimental and theoretical values. An example is the filling of the secondary coil inner volume, where in an ideal case, volume must be filled completely to obtain precision in the magnetization magnitude value. In experimentation, the sample holder thickness and the coils spool thickness avoid this inner volume to be filled completely. In this measurements the sample magnetization magnitude was not calibrated in order to obtain validated magnetization magnitude values. In addition to, each set of measurements needs a proper calibration until the system possesses a correct robustness.

Finally, is important to note that the signal-to-noise ratio decreases as the frequency increases. Because of the output voltage dependence on frequency, it is expected to obtain an increase of output voltage magnitude due to the magnetization. In addition to, the imbalance signal of the output voltage should always increase proportionally to the frequency, which is not the actual case. However,

changes in the voltage signal can be observed when the sample moves between the two coils of the first-order gradiometer, and from which results can be obtained.

3.2 FERROFLUIDS

3.2.1 Particle synthesis and characterization

The ferrofluids consisted of cobalt ferrite $CoFe_2O_4$ nanoparticles synthesized by thermal decomposition using 1-octadecene as solvent. At this point, 25 g of an iron-cobalt oleate were reacted with 100 ml of 1-octadecene and 2 g of oleic acid. The reaction was carried out at 320 °C for 3 h, in which a heating rate of 3.5 °C/*min* was used to increase temperature up to 320 °C. The mixture was cooled to room temperature and washed three times with acetone (1:3) at 8000 rpm for 15 min. Figure 3-8 shows narrow size distribution of about 14.0 ± 2.0 nm, determined by Transmission Electron Microscopy (TEM) using a JEOL 1200EX. A mean hydrodynamic diameter of 23.1nm was determined by Dynamic Light Scattering (DLS) (Figure 3-9). Because the intensity distribution is very sensitive to the light scattered by larger nanoparticles, the volume distribution shows accurately the existence of a group of 170nm nanoparticles, corresponding to aggregates, is not presented in volume analysis.

Suspension. The nanoparticles were suspended in four mixtures of mineral oil and hexane, 25%w/w hexane-75%w/w mineral oil, 50%w/w hexane-50%w/w mineral oil, 75%w/w hexane-25%w/w mineral oil, 100%w/w hexane. The approximate particle concentration in the ferrofluids was 15%w/w as determined using thermogravimetric analysis (TGA). A particle concentration of 15%w/w provides curves with less noise. Higher particle concentrations could saturate the INamp and increase the particle-particle interaction, which is not desirable. Although lower particle concentration decreases the particle-particle interaction, the noise increases due

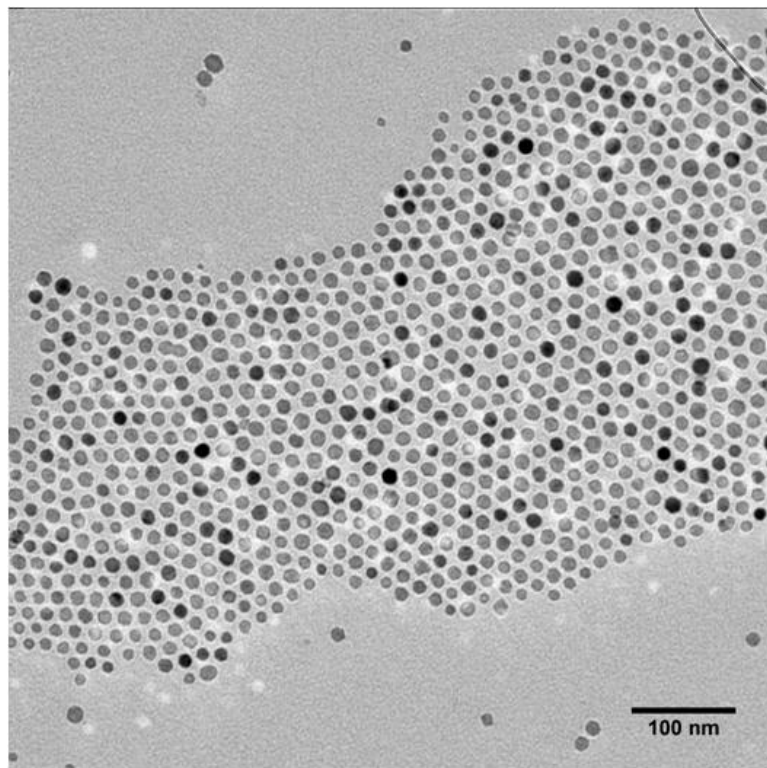


Figure 3–8: Transmission Electron Microscope (TEM) of cobalt ferrite nanoparticles. A size and narrow size distribution of about 14.0 ± 2.0 nm was obtained.

to a low signal-to-noise ratio. From the magnetization curve (Figure 3-10), the initial magnetic susceptibility for these samples could be obtained using the slope at the linear region. The initial magnetic susceptibility was 1.35×10^5 .

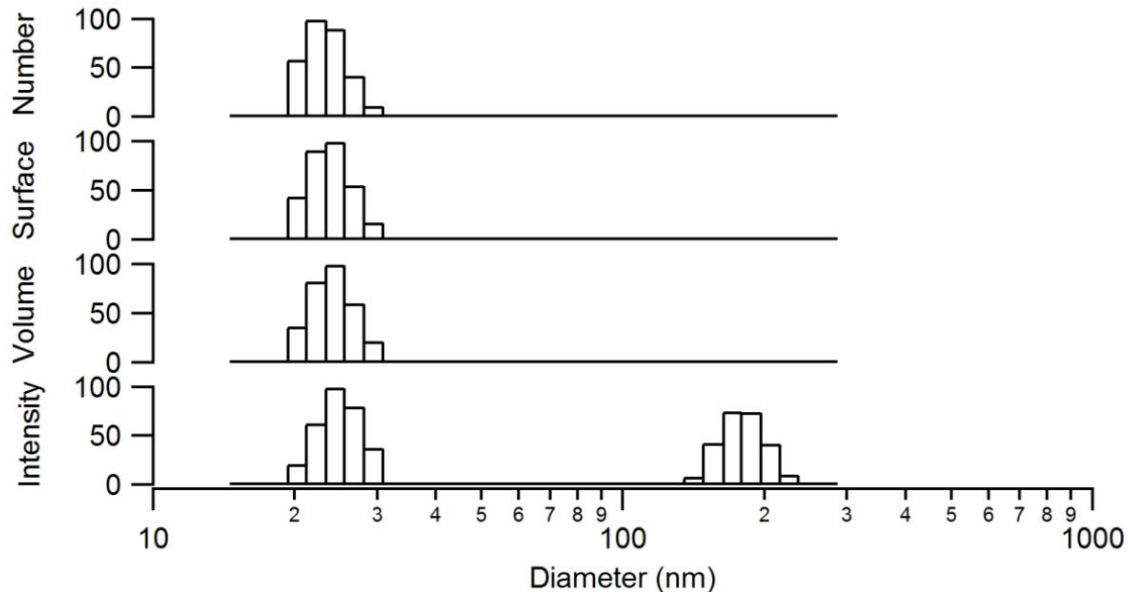


Figure 3-9: Dynamic Light Scattering (DLS) of cobalt ferrite ferrofluid. A mean hydrodynamic diameter of 23.1nm is observed in three different analysis. The intensity measurement, which is commonly used to report the size of each peak in the distribution, shows two groups of nanoparticles sizes, where a group with an approximately size of 170nm has a magnitude similar to those with a size of 23.1nm.

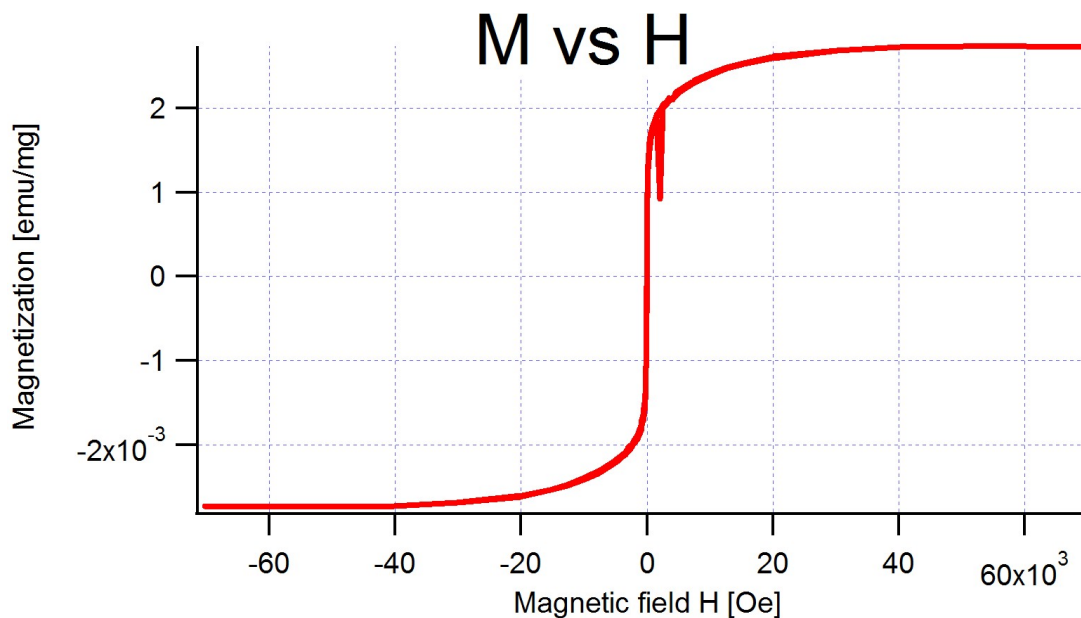


Figure 3-10: Magnetization versus magnetic field for $CoFe_2O_4$ nanoparticles suspended in hexane with a concentration of 15%w/w. The initial magnetic susceptibility was 1.35×10^5 as determined from the slope at the linear region.

CHAPTER 4

RESULTS

This chapter presents the results from exposing the cobalt ferrite ferrofluid to the AC magnetic field generated in the primary coil and measuring its magnetization with the first-order gradiometer as the secondary, from which a frequency sweep of the complex magnetic susceptibility is obtained.

4.1 Data and analysis of complex magnetic susceptibility

The curves obtained for each suspension are presented. For each frequency in each actuator position, a quantity of 100 measurements were used to calculate a mean value. The curves were normalized with respect to the maximum value obtained from the four suspensions.

Figure 4-1 presents the real and imaginary parts of the magnetic susceptibility of the cobalt ferrite nanoparticles suspended in hexane.

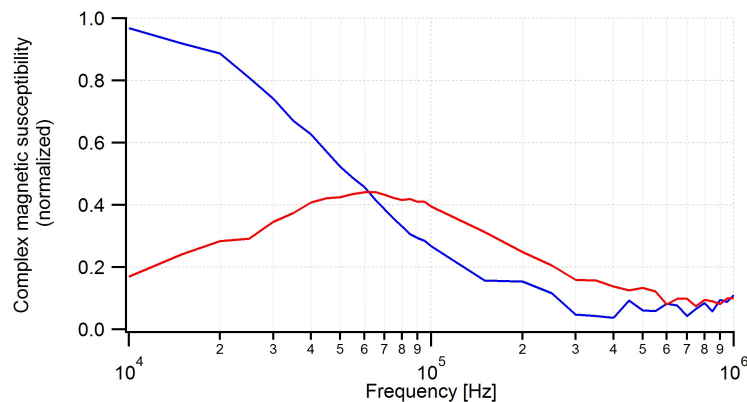


Figure 4-1: Complex magnetic susceptibility of the cobalt ferrite nanoparticles suspended in hexane. The maximum value of χ'' is observed at a frequency of $f = 65\text{kHz}$.

In Figure 4-1, the maximum value of χ'' is observed at a frequency of $f = 65\text{kHz}$, which is in good agreement with the theoretical Debye model where χ'' is almost half the value of χ_0 , as predicted in theory, and the χ'' peak intersects with the χ' curve. Some noise is observed at frequencies over 300kHz . This noise could be a signal-to-noise ratio problem, caused by an increase of the imbalance signal, which is proportional to frequency.

Figure 4-2 presents the real and imaginary parts of the magnetic susceptibility of the cobalt ferrite nanoparticles suspended in a mixture of 75%w/w hexane-25%w/w mineral oil.

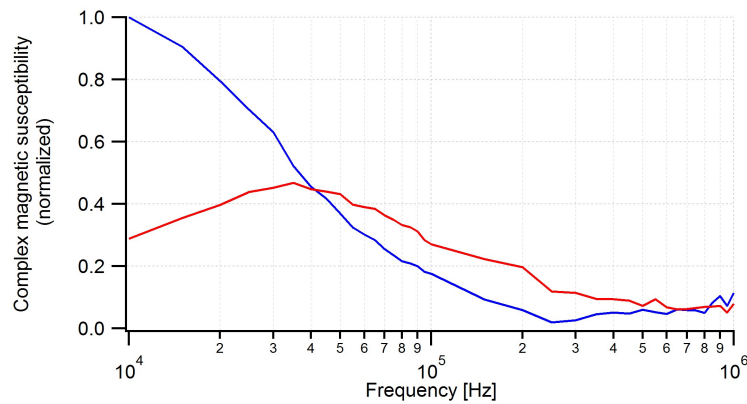


Figure 4–2: Complex magnetic susceptibility of the cobalt ferrite nanoparticles suspended in a mixture of 75%w/w hexane-25%w/w mineral oil. The maximum value of χ'' is observed at a frequency of $f = 35\text{kHz}$.

Figure 4-2, as well as in Figure 4-1, presents a curve which is similar to the ideal Debye model. Although lower noise is observed in this curve, the value of χ' is closer to be half of the χ_0 value. In addition to, an important observation is that the magnitude of χ'' , in where intersects with χ' , is shortly shifted in comparison to the one observed in the Figure 4-1.

Figure 4-3 presents the real and imaginary parts of the magnetic susceptibility of the cobalt ferrite nanoparticles suspended in a mixture of 50%w/w hexane-50%w/w mineral oil.

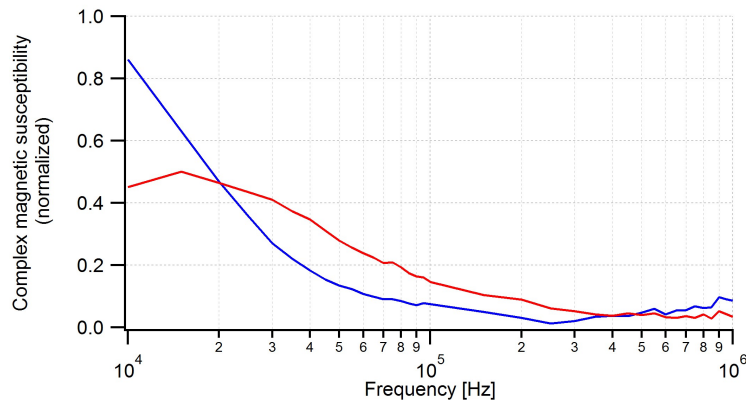


Figure 4–3: Complex magnetic susceptibility of the cobalt ferrite nanoparticles suspended in a mixture of 50%w/w hexane-50%w/w mineral oil. The maximum value of χ'' is observed at a frequency of $f = 15\text{kHz}$.

The curve in Figure 4-3 presents very similar characteristic to the one of Figure 4-4, in where the value of χ' is even closer to be half of the χ_0 value and the $\chi' - \chi''$ intersection is farther from the χ'' peak.

Figure 4-4 presents the real and imaginary parts of the magnetic susceptibility of the cobalt ferrite nanoparticles suspended in a mixture of 25%w/w hexane-75%w/w mineral oil.

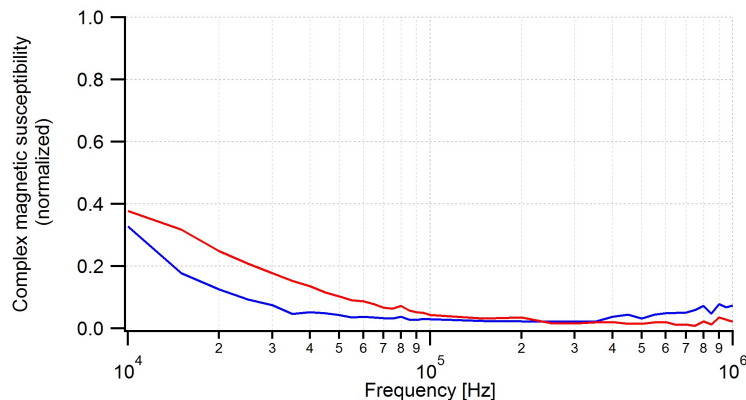


Figure 4–4: Complex magnetic susceptibility of the cobalt ferrite nanoparticles suspended in a mixture of 25%w/w hexane-75%w/w mineral oil. The maximum value of χ'' cannot be observed precisely, but exists below $f = 10\text{kHz}$.

The χ'' peak cannot be observed in Figure 4-4, although the behavior is similar to the expected for values after the χ'' peak.

Finally, Figure 4-5 shows the complex magnetic susceptibility of all suspension in order to compare the behavior of the curves.

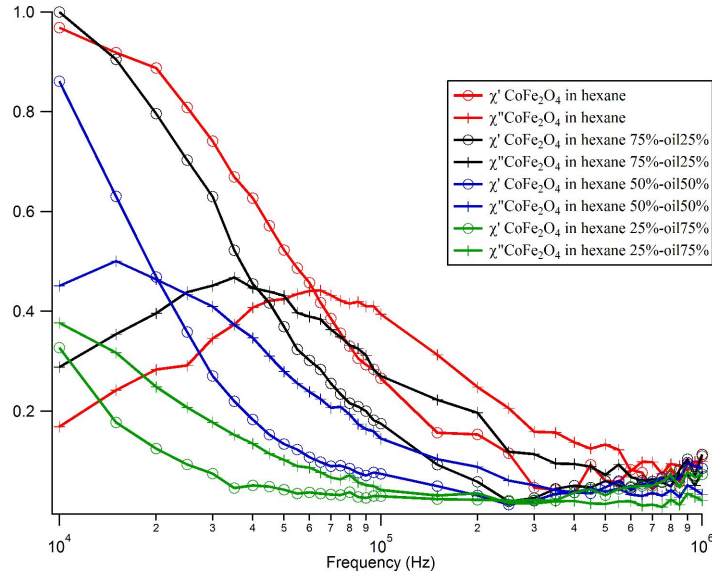


Figure 4-5: Complex magnetic susceptibility of the cobalt ferrite nanoparticles suspended in mixtures of 25%w/w hexane-75%w/w mineral oil, 50%w/w hexane-50%w/w mineral oil, 75%w/w hexane-25%w/w mineral oil, 100%w/w hexane. It can be observed that maximum value for χ'' varies to higher frequencies as the viscosity of carrier fluid decreases.

As expected from theory, the suspension with lower viscosity shows the χ'' peak at higher frequencies. Next section compares the carrier fluid viscosity obtained from two methods, the magnetization method and the capillary viscometer.

4.2 Viscosity measurements and comparison with values obtained from complex magnetic susceptibility

Results of the viscosity obtained from the complex magnetic susceptibility measurements and from capillary viscometer are tabulated and presented in Table 4-1. Although the AC magnetic susceptometer lacks of temperature control, the measurements with the viscometer were made in a controlled water bath at 25 °C (room temperature) in order to obtain the most accurately conditions as the AC magnetic susceptometer environment.

From table 4-1, it can be observed that viscosities derived from the complex magnetic susceptibility overestimate the values obtained from validated method.

Considering the most reliable result (not the values from the 25%w/w hexane-75%w/w mineral suspension), the relative difference increase at lower viscosities. This can be observed by estimating theoretically the frequency for which the χ'' peak must appear.(Table 4-2)

Table 4-1: Comparison between the viscosity obtained from complex magnetic susceptibility and capillary viscometer

	Frequency of χ'' max value [kHz]	Viscosity from complex magnetic susceptibility [cP]	Viscosity from viscometer [cP]
hexane25%-oil75%	10	<i>a</i>	4.46
hexane50%-oil50%	15	2.28	1.52
hexane75%-oil25%	35	0.978	0.553
hexane	60	0.571	0.294 ^b

^a Value less than 10kHz. Out of the instrument's frequency range.

^b Data from literature

Table 4-2: Estimation and comparison between the frequency in where the maximum χ'' value was expected with and the experimental frequency

	Validated viscosity [cP]	Expected frequency [kHz]	Experimental frequency [kHz]	Frequency ratio [kHz/kHz]
hexane25%-oil75%	4.46	7.579	<10	<i>N/A</i>
hexane50%-oil50%	1.52	22.239	15	1.483
hexane75%-oil25%	0.553	61.127	35	1.746
hexane	0.294 ^b	114.977	60	1.916

4.3 Discussion

Differences in results could be caused by any of the following: particle-particle interactions such as friction and aggregation, temperature, or system sensitivity. Although negligible quantity of aggregation was observed in the DLS results, aggregations which simulates larger particles are considered because theoretically, a larger particle contributes more to the magnetization and the dynamic of the fluid

than a small particle. High ferrofluid concentration also affects the measurements because the distance between the particles will be closer, leading to interaction between the particles instead of interactions with the solvent. The temperature is a very important factor affecting the viscosity of the fluid. Although the AC magnetic susceptometer lacks temperature control, the measurements with the viscometer were made in a controlled water bath at 25 °C (room temperature). Even though there was not a big difference in temperature for both case, it can be seen that the Brownian relaxation time is inversely proportional to temperature, in which changes in temperature affect directly the dynamic of the nanoparticles. In addition to, the viscosity is also an function of temperature. As the temperature increases, the viscosity decreases, consequently contributing to the decrease of the relaxation time. Finally, the lack of very good sensitivity, as could be reached by SQUIDs, could be affecting the measurement of sample magnetization. This happens because of a reduction of signal-to-noise ratio due to the increase of the imbalance signal when the frequency increase. System sensitivity must be improved in order to overtake the effect caused by the low signal-to-noise ratio.

CHAPTER 5

CONCLUSION AND RECOMMENDATIONS

An AC susceptometer was developed, in which features such as the coils design and a high speed instrumentation amplifier allow the instrument to realize measurements in the improved frequency range of 10kHz-1MHz with a constant excitation field of approximately 4.25 Oe. Design considerations for the high frequency ranges such as the increase of wire insulator and the development of a high speed instrumentation amplifier using voltage feedback LM7171, allow a successful performance of the instrument. LabView software was used to automate the instrument. In order to validate the AC susceptometer, viscosities of magnetic colloids carrier fluid were calculated by means of complex magnetic susceptibility and capillary viscometer, and whose values present minimum differences. Differences between theoretical and experimental values increase as the frequency of χ'' peak value increases, coincident with the proportional decrease of the signal-to-noise ratio which avoids precision in the measurement of the in-phase and out-of-phase components. Particle-particle interactions may be affecting the dynamics of the particles in the solvent, which could lead to higher relaxation times. In addition to, limitation in temperature control and system sensitivity affect the magnetization measurements.

In order to improve the system for future work, the temperature control must be implemented to maintain a constant temperature across the sample during the measurements. A thoughtful temperature control design is required to avoid unwanted temperatures in the wire conductor. It is recommended to fix temperature in the primary and the secondary in order to avoid variations in the conductor resistance

and prevent heat transfer to the sample due to high current through the conductor. In addition to heating effect in the conductor due to current density, skin effect will be affecting the conductor temperature if a constant current is maintained constant while the frequency is increased. For ease the implementation process for the coils temperature, both coils could be exposed to the same temperature source, but must be different from the sample temperature source. Liquid helium or liquid hydrogen are good options to use as temperature controlled medium. In addition to, high system sensitivity is mandatory to improve even more the frequency range. A good option to extend the frequency range to lower frequencies is the design a high speed instrumentation amplifier with higher gain while reducing the secondary turns to avoid saturation at high frequencies. A better option will be to use a lock-in amplifier which works in the frequency range desired. It will be always good to use an oscilloscope to observe if there is sufficient signal-to-noise ratio. Probably, the best option is to implement a SQUID to achieve very high sensitivity. Also, a similar experiment could be done with particles suspended in a single fluid or homogeneous fluid in order to promote the particle-solvent interaction to be the same for all the nanoparticles. An experiment with lower concentration of particles is important to avoid the effect caused by the particle-particle interactions. Finally, a calibration constant must be calculated to obtain absolute magnitude values. This errors in magnitude due to imperfections in construction could be corrected by comparing magnetization magnitude per mass at 1kHz obtained from the Quantum Design MPMS with the magnetization magnitude per mass obtained at the initial frequency of the AC magnetic susceptometer. Dysprosium oxide must be used to as standard sample to calibrate the phase and magnitude, and to obtain the magnitude constant for the absolute values.

APPENDIX A

DERIVATION OF EQUATIONS

A.1 Mathematical description of the generation of a magnetic field and the magnetic field intensity at any point of a non-infinite coil [2]

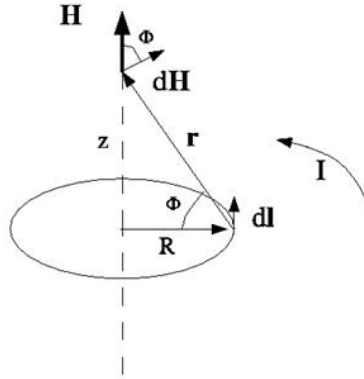


Figure A-1: Diagram of a current loop generating a magnetic field used as a representation of the Biot-Savart's law

The generation of a magnetic field \mathbf{H} established for a current element I is described by the Biot-Savart's law which is expressed in vector form as

$$d\mathbf{H} = \frac{I d\mathbf{l} \times \mathbf{r}}{4\pi r^3}. \quad (\text{A.1})$$

In the case of one current loop, the equation for magnetic field intensity is

$$\mathbf{H} = \frac{IR^2 \mathbf{a}_n}{4\pi r^3} \quad (\text{A.2})$$

where \mathbf{a}_n is the direction normal to the center loop face. Refer to Figure A-1 for conceptual details. Now, considering N number of current loops as in the case of the coil in Figure A-2, the intensity of magnetic field at any point in the z axis is given by

$$\mathbf{H} = \frac{NI}{2l} (\cos \theta_2 - \cos \theta_1) \mathbf{a}_z. \quad (\text{A.3})$$

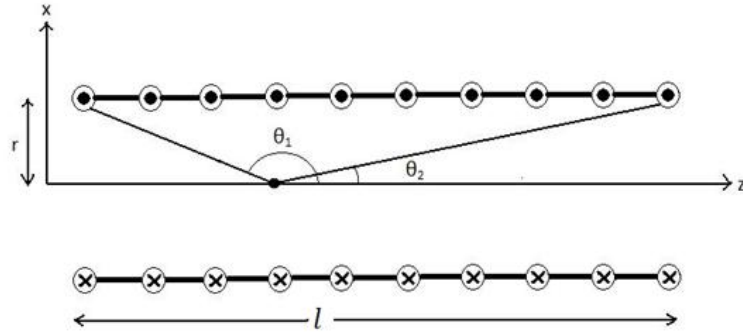


Figure A-2: Magnetic field intensity inside the central axis of a coil

Assuming an infinite length coil, Equation A.4 reduces to

$$\mathbf{H} = \frac{NI}{l}. \quad (\text{A.4})$$

A.2 Output voltage of a secondary coil with a symmetric first-order gradiometer configuration

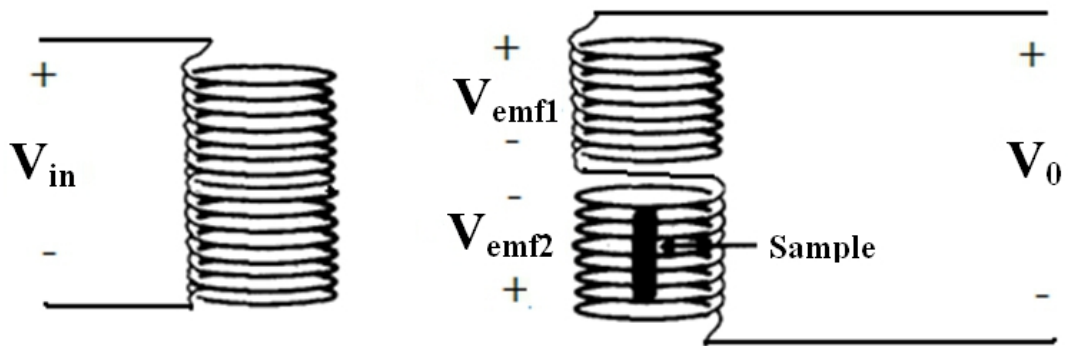


Figure A-3: Diagram of a primary and secondary coil configuration. The sample is assumed to exist in the lower coil of the secondary.

Symbols used for this derivation:

Ψ	Total magnetic flux.
\mathbf{B}	Magnetic flux density.
\mathbf{S}	Surface area.
V_{emf1}	Induced voltage in the upper coil in the secondary.
V_{emf2}	Induced voltage in the lower coil in the secondary.
N_1	Number of turns in the primary.
N_{21}	Number of turns in the upper coil of the secondary.
N_{22}	Number of turns in the lower coil of the secondary.
A_{21}	Area of the upper coil of the secondary.
A_{22}	Area of the lower coil of the secondary.
$i(t)$	Current through the primary.
χ_m	Magnetic susceptibility of the sample.

- L_1 Length of the primary.
 μ Permeability of the material.

Using the following equations, the output voltage of the secondary coil can be obtained. It is considered the changes in permeability of the secondary inner coil volume.

From the Faraday's law of induction, an output voltage due to an induced magnetic field can be obtained.

$$V_{emf} = -N \frac{d\Psi}{dt} \quad (\text{A.5})$$

The magnetic flux through an enclosed surface is given by

$$\Psi = \int_S \mathbf{B} \cdot d\mathbf{S} = BA \quad (\text{A.6})$$

with an area $A = \pi r^2$ perpendicular to the magnetic flux lines, and a magnetic flux density \mathbf{B} . The magnetic flux density is related to the magnetic field intensity \mathbf{H} in the following equation given by

$$\mathbf{B} = \mu \mathbf{H} \quad (\text{A.7})$$

in where μ is the permeability of the material. The magnetic susceptibility can be obtained from its relationship with the permeability, which is given by

$$\mu = \mu_0(\chi_m + 1). \quad (\text{A.8})$$

The derivation of the output voltage equation is as follows:

$$V_{emf2} = -N_{22} \frac{d\Psi}{dt} \quad (\text{A.9})$$

$$V_{emf2} = -N_{22} \frac{d}{dt} \mathbf{B} A_{22} \quad (\text{A.10})$$

$$V_{emf2} = -N_{22} \frac{d}{dt} \frac{\mu N_1 i(t) A_{22}}{L_1} \quad (\text{A.11})$$

$$V_{emf2} = -\frac{N_{22} N_1 A_{22}}{L_1} \frac{d}{dt} \mu i(t) \quad (\text{A.12})$$

$$V_{emf2} = -\frac{N_{22} N_1 A_{22}}{L_1} \frac{d}{dt} \mu_0 (\chi_m + 1) i(t) \quad (\text{A.13})$$

$$V_{emf2} = -\frac{\mu_0 N_{22} N_1 A_{22}}{L_1} \frac{d}{dt} (|\chi_m| e^{j(\theta_\chi)} + 1) |I| e^{j(\omega t + \theta_I)} \quad (\text{A.14})$$

$$V_{emf2} = -\frac{\mu_0 N_{22} N_1 A_{22} |I|}{L_1} \frac{d}{dt} (|\chi_m| e^{j(\omega t + \theta_\chi + \theta_I)} + e^{j(\omega t + \theta_I)}) \quad (\text{A.15})$$

The sample will be present only in one coil of the secondary. Let's assume that there is no sample in the upper coil, therefore $|\chi_m| = 0$.

$$V_{emf1} = -\frac{\mu_0 N_{21} N_1 A_{21} |I|}{L_1} \frac{d}{dt} (e^{j(\omega t + \theta_I)}) \quad (\text{A.16})$$

$$V_0 = V_{emf1} - V_{emf2} \quad (\text{A.17})$$

$$V_0 = \left[-\frac{\mu_0 N_{21} N_1 A_{21} |I|}{L_1} \frac{d}{dt} (e^{j(\omega t + \theta_I)}) \right] - \left[-\frac{\mu_0 N_{22} N_1 A_{22} |I|}{L_1} \frac{d}{dt} (|\chi_m| e^{j(\omega t + \theta_\chi + \theta_I)} + e^{j(\omega t + \theta_I)}) \right] \quad (\text{A.18})$$

$$V_0 = \left[-j \frac{\mu_0 \omega N_{21} N_1 A_{21} |I|}{L_1} (e^{j(\omega t + \theta_I)}) \right] - \left[-j \frac{\mu_0 \omega N_{22} N_1 A_{22} |I|}{L_1} (|\chi_m| e^{j(\omega t + \theta_\chi + \theta_I)} + e^{j(\omega t + \theta_I)}) \right] \quad (\text{A.19})$$

Assuming $A_{21} = A_{22} = A_2$

$$V_0 = j \frac{\mu_0 \omega N_1 A_2 |I|}{L_1} (-N_{21} e^{j(\omega t + \theta_I)} + N_{22} |\chi_m| e^{j(\omega t + \theta_x + \theta_I)} + N_{22} e^{j(\omega t + \theta_I)}) \quad (\text{A.20})$$

$$V_0 = j \frac{\mu_0 \omega N_1 A_2 |I|}{L_1} e^{j(\omega t + \theta_I)} (-N_{21} + N_{22} |\chi_m| e^{j(\theta_x)} + N_{22}) \quad (\text{A.21})$$

Assuming $N_{21} = N_{22} = N_2$

$$V_0 = j \frac{\mu_0 \omega N_2 N_1 A_2 |\chi_m| |I|}{L_1} (e^{j(\omega t + \theta_I + \theta_x)}) \quad (\text{A.22})$$

$$V_0 = \frac{\mu_0 \omega N_2 N_1 A_2 |\chi_m| |I|}{L_1} (e^{j(\omega t + \theta_I + \theta_x + 90^\circ)}) \quad (\text{A.23})$$

APPENDIX B

SUMMARY OF LABVIEW OPERATION

This chapter explains a brief summary of the LabVIEW programming and operation when the measurements were taken.

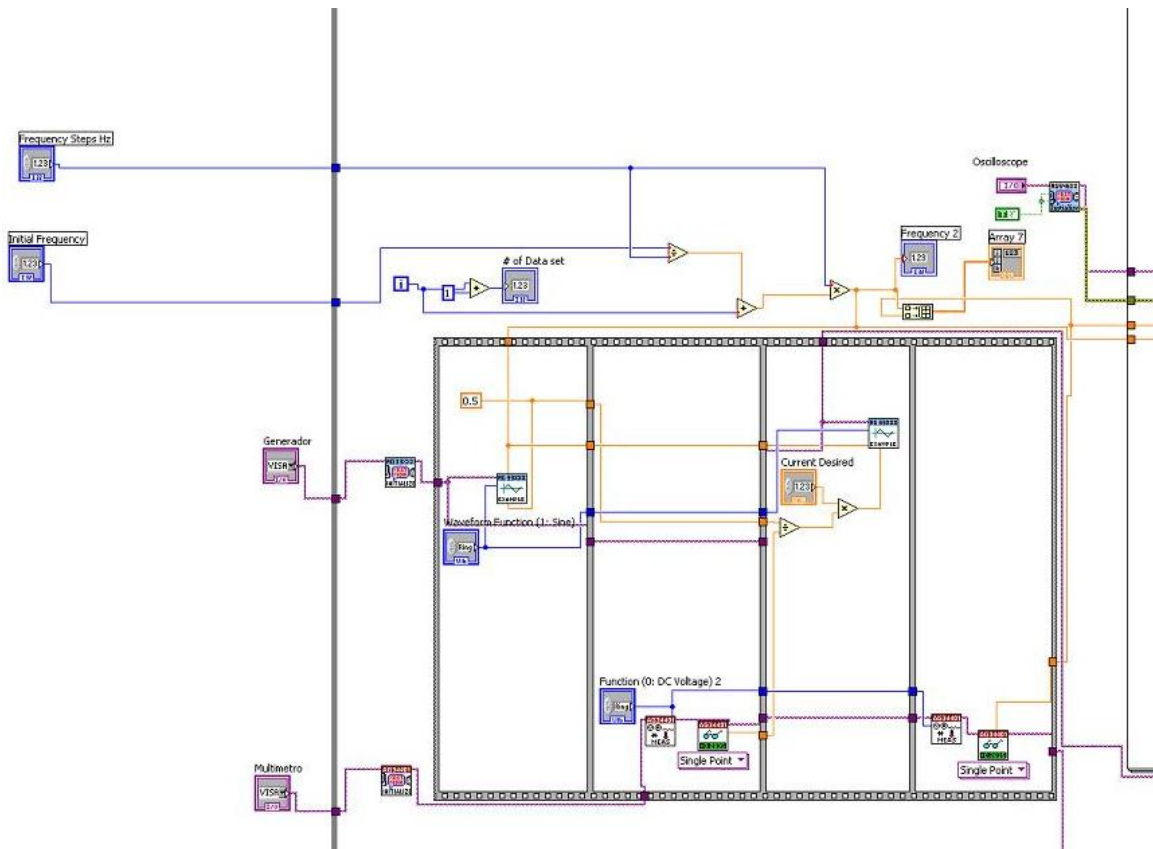


Figure B-1: Program to setup the magnetic field intensity

Figure B-1 presents the program used to set the magnetic field intensity. For any random voltage, the current is measured using the multimeter. Using the value of voltage and current, the impedance is obtained. Now, the voltage is increased

to obtain a current value of 1 A, which gives a magnetic field intensity of approximately 4.25 Oe. This is measured at each frequency because of the impedance changes while the frequency increases.

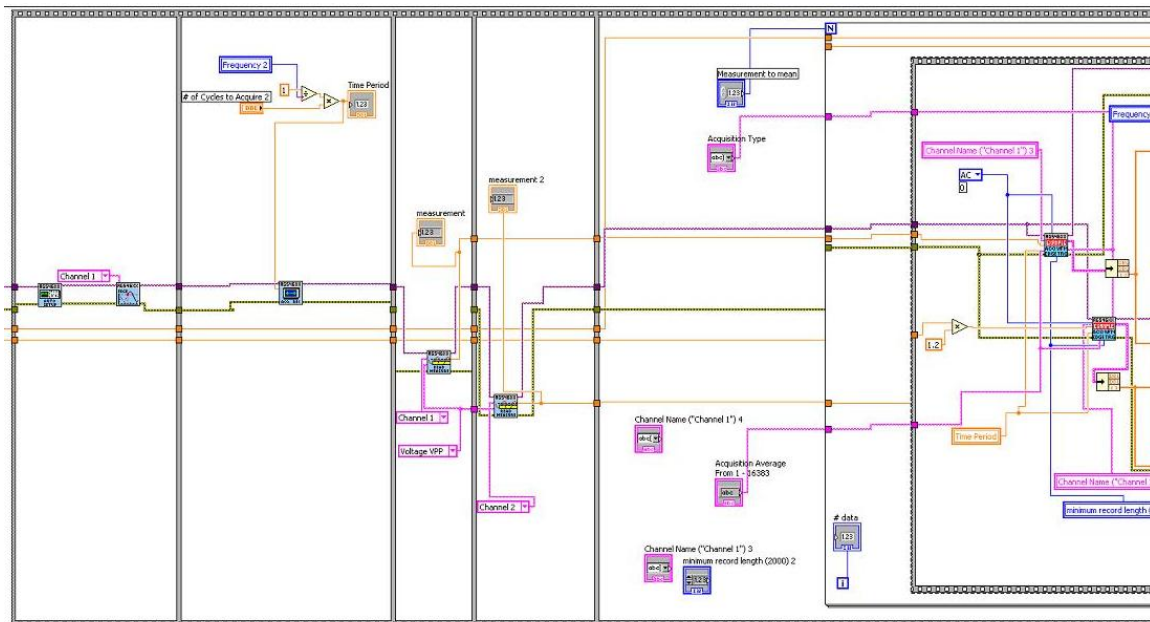


Figure B-2: Oscilloscope setup and data acquisition program

Figure B-2 shows the program section where the oscilloscope is set and the acquisition is performed. The oscilloscope autoscale is initially used. The signal amplitude for both channels is measured to adjust the scale to the most appropriate. Using the frequency sent to the signal generator, the time scale is adjusted to obtain four cycles. After the signals are acquired, they are passed through a 10th order low-pass filter.

Figure B-3 shows the a program which selects a signals section used to ease the search of the in-phase and out-of-phase values. The signals selection is from $-\pi/10$ to $3/10\pi$, which includes the 0° and 90° of the primary signal. From the selected signals, the minimum and maximum absolute values of the primary, which are 0° and 90° respectively, was obtained to use their indexes and find the in-phase and out-of-phase values in the secondary signal.

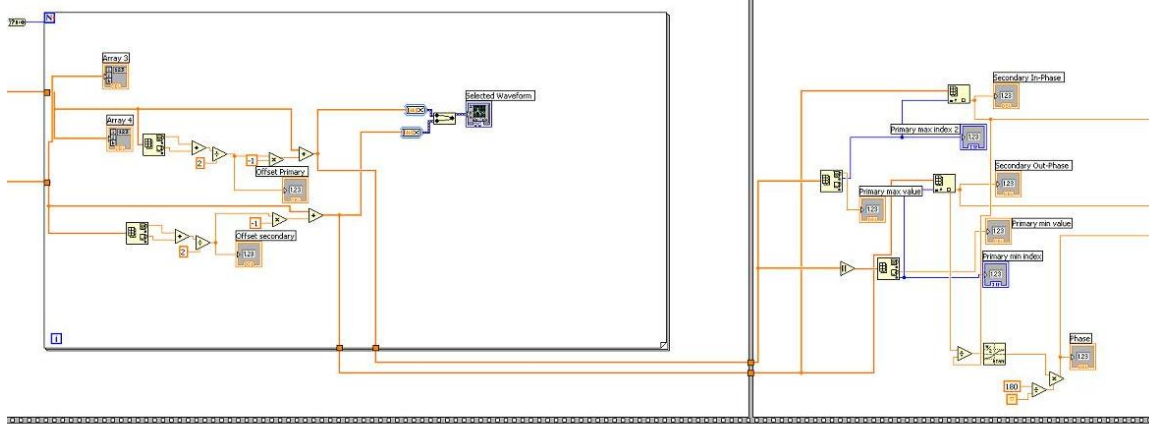


Figure B-3: Program to select the waveform used to obtain the in-phase and out-of-phase values

Finally, after the data was obtained, the motor moves the sample between the upper and lower coil of the secondary. Instructions were used as defined in the motor's user manual, and are sent through serial communication. The motor was set to move 50mm, which corresponds to the distance between the upper and lower coil.

REFERENCE LIST

- [1] QuantumDesign, "**Introduction to: AC Susceptibility**". San Diego, California. U.S.A. 92121-1311
- [2] Matthew N. O. Sadiku, "**Elements of electromagnetic**", Third edition. New York: Oxford University Press, INC, 2001
- [3] www.imego.com
- [4] de Souza, R. R., and C. J. Magon. "**A moving coil ac magnetic susceptometer.**", *Review of scientific instruments*, Feb. 1998: Vol 69, 2, Pag. 431-436.
- [5] Ramakrishnan, S, S Sundaram, R S Pandit, and Girish Chandra. "**An AC susceptometer from 1.5 to 300k.**", *J. Phys. E: Sce. Instrum*, Vol. 18, 1985: Pag. 650-653.
- [6] Maxwell, E., "**Mutual Inductance Bridge for ac Susceptibility Measurements at Low Frequencies**", *Review of Scientific Instruments*, Vol. 36, p.553-554
- [7] Anderson, A. C., "**Measurements of Demagnetizing Factors and Their Application to Magnetic Thermometry**", *J. Appl. Phys.*, v.39, pag.5878, Dec. 1968
- [8] Anderson, A. C.; Peterson, R. E.; Robichaux, J. E., "**Magnetic Thermometry**", *Review of Scientific Instruments*, Vol. 41, Issue: 4, pag. 528 - 532, Apr. 1970
- [9] Zoya; Popovic, Branko D., Popovic, "**Introductory Electromagnetics Popovic**". Prentice-Hall, Inc. Upper Saddle River, New Jersey 07458. 2000
- [10] www.tristantech.com

- [11] P C Fannin, S W Charles and T Relihan. "**Broad-band measurement of the complex susceptibility of magnetic fluids.**", *Meas. Sci. Technol.*, Jul. 1993: v.4 , pag.1160-1162.
- [12] P.C. Fannin, C. MacOireachtaigh, C. Couper. "**An improved technique for the measurement of the complex susceptibility of magnetic colloids in the microwave region.**", *Journal of Magnetism and Magnetic Materials*, Mar. 2010: v.322, pag.2428-2433.
- [13] P C Fannin, B K P Scaif and S W Charles. "**New technique for measuring the complex susceptibility of ferrofluids.**", *J. Phys. E: Sci. Instrum.: Rapid communications*, 1986: v.19, pag.238-239.
- [14] P.C. Fannin, D. Vincent, G. Noyel. "**On the measurement of the complex susceptibility and permittivity of magnetic fluids by means of two different measurement techniques.**", *Journal of Magnetism and Magnetic Materials*, 1999: v.201, pag.116-118.
- [15] J.-C. Bacri, J. Dumas, D. Gorse, R. Perzynski and D. Salin. "**Ferrofluid viscometer.**", *J. Physique Lett.*, Dec. 1985: v.46,pag.1199-1205.
- [16] Seok-Hwan Chung, Marcos Grimsditch, Axel Hoffmann, Samuel D. Bader, Jin Xie, Sheng Peng, Shouheng Sun. "**Magneto-optic measurement of Brownian relaxation of magnetic nanoparticles.**", *Journal of Magnetism and Magnetic Materials*, May. 2007: v.320 ,pag.91-95.
- [17] Nikolo, Martin. "**Superconductivity: A guide to alternating current susceptibility measurements and alternating current susceptometer design.**", *American Journal of Physics*, Jan. 1985: v.63,pag.57-65.
- [18] Roque, A., J. Maia, E. Margato, D.M. Sousa, and G.D. Marques. "Characterization of the Fringing Window of a magnetic core." EUROCON - International Conference on Computer as a Tool (EUROCON), 2011 IEEE . Lisbon, 27-29 April 2011 . 1-4 .

- [19] M. J. Martinez-Prez, J. Ses, F. Luis, D. Drung, and T. Schurig. "**Note: Highly sensitive superconducting quantum interference device microsusceptometers operating at high frequencies and very low temperatures inside the mixing chamber of a dilution refrigerator.**", *Review of Scientific Instruments*, Jan. 2010: v.81 .
- [20] M. Marinelli, B. Gianesin, M. Lamagna, A. Lavagetto, E. Oliveri, M.L. Saccone, G. Sobrero, L. Terenzani, G.L. Forni. "**Whole liver iron overload measurement by a non cryogenic magnetic susceptometer.**", *International Congress Series*, 2007: v.1300, pag.299-302.
- [21] J A Overweg, H J M ter Brake, J Flokstra and G J Gerritsma. "**An automatic frequency-sweeping SQUID susceptometer.**", *J. Phys. E: Sci. Instrum.*, 1983: v.16, pag.1247-1253.
- [22] A. D. Hibbs, R. E. Sager, S. Kumar, J. E. McAtthur, and A. L. Singsaas, K. G. Jensen, M. A. Steindorf, T. A. Aukerman, and H. M. Schneider. "**A SQUID-based ac susceptometer.**" *Rev. Sci. Instrum.*, Aug.1994: v.65, pag.2644-2652.
- [23] Cor, L.A.; Romeiro, F.G.; Stelzer, M.; Amrico, M.F.; Oliveira, R.B.; Baffa, O.; Miranda, J.R.A., "**AC biosusceptometry in the study of drug delivery**", *Advanced Drug Delivery Reviews*, v 57, n 8, p 1223-1241, June 15, 2005
- [24] Kashevsky, Bronislav E.; Agabekov, Vladimir E.; Kashevsky, Sergei B.; Kekalo, Katsiaryna A.; Manina, Elena Yu.; Prokhorov, Igor V.; Ulashchik, Vladimir S., "**Study of cobalt ferrite nanosuspensions for low-frequency ferromagnetic hyperthermia**", *Particuology*, v 6, n 5, p 322-333, October 2008
- [25] Namdeo, Mini; Saxena, Sutanjay; Tankhiwale, Rasika; Bajpai, M.; Mohan, Y.M.; Bajpai, S.K., "**Magnetic nanoparticles for drug delivery applications**", *Journal of Nanoscience and Nanotechnology*, v 8, n 7, p 3247-3271, July 2008

- [26] Wilhelm, Claire; Gazeau, Florence, "**Magnetic nanoparticles: Internal probes and heaters within living cells**", *Journal of Magnetism and Magnetic Materials*, v 321, n 7, p 671-674, April 2009
- [27] Bajkowski, J.; Nachman, J.; Shillor, M.; Sofonea, M., "**A model for a magnetorheological damper**", *Mathematical and Computer Modelling*, v 48, n 1-2, p 56-68, July 2008
- [28] Zarina Bhimani, "**Ferrofluidic sealing**"; Article, Ferrotec Corp, Nashua, New Hampshire, USA, July 2002
- [29] Nakatsuka, K.; Jeyadevan, B.; Neveu, S.; Koganezawa, H., "**The magnetic fluid for heat transfer applications**", *Journal of Magnetism and Magnetic Materials*, v 252, n 1-3 SPEC. ISS., p 360-362, November 2002
- [30] www.britannica.com
- [31] Fannin, P.C., "**Characterisation of magnetic fluids**", *Journal of Alloys and Compounds*, v 369, n 1-2, p 43-51, April 28, 2004
- [32] Rinaldi, Carlos; Chaves, Arlex; Elborai, Shihab; He, Xiaowei; Zahn, Markus, "**Magnetic fluid rheology and flows**", *Current Opinion in Colloid and Interface Science*, v 10, n 3-4, p 141-157, October 2005
- [33] B. Fischer, B. Huke, M. Lcke, R. Hempelmann, "**Brownian relaxation of magnetic colloids**", *J. Mag and Magnetic Mat.*, Nov. 2004: v.289,pag.74-77.
- [34] Kopcansk, Peter; Timko, Milan; Potocov, Ivana; Konerack, Martina; Jurkov, Alena; Tomaovicov, Natlia; telina, Jlius; Musil, Ctibor; Bracink, Juraj, "**The determination of the hydrodynamic diameter of magnetic particles using FRS experiment**", *Journal of Magnetism and Magnetic Materials*, v 289, p 97-100, March 2005, Proceedings of the 10th International Conference on Magnetic Fluids
- [35] Victoria L. Calero-DdelC, Darlene I. Santiago-Quionez and Carlos Rinaldi. "**Quantitative nanoscale viscosity measurements using magnetic**

- nanoparticles and SQUID AC susceptibility measurements.”, *The Royal Society of Chemistry: Soft Matter*, Jan. 2011: v.7, pag.4497-4503.
- [36] Suto, Makoto; Hirota, Yasutake; Mamiya, Hiroaki; Fujita, Asaya; Kasuya, Ryo; Tohji, Kazuyuki; Jeyadevan, Balachandran, ”**Heat dissipation mechanism of magnetite nanoparticles in magnetic fluid hyperthermia**, *Journal of Magnetism and Magnetic Materials*, v 321, n 10, p 1493-1496, May 2009
- [37] William D. Callister,Jr., ”**Materials science and engineering an introduction**”, Sixth edition. New York: John Wiley and Sons, Inc, 2003.
- [38] Randall D. Knight, ”**Physics for scientists and engineers: A strategic approach**”, Pearson Education INC., 2004
- [39] knol.google.com/k/mems-fabrication-process
- [40] www.feppd.org
- [41] info.ee.surrey.ac.uk/Workshop/advice/coils/mu/
- [42] hyperphysics.phy-astr.gsu.edu/hbase/solids/hyst.html
- [43] www.irm.umn.edu/hg2m/hg2m_b/hg2m_b.html
- [44] Granger, Robert Alan, ”**Fluid Mechanics**”. Mineola, New York: Dover Publication, INC, 1985, 1995
- [45] J. R. Van Wazer, J. W. Lyons, K. Y. Kim, and R. E. Colwell, ”**Viscosity and Flow Measurement: A Laboratory Handbook of Rheology**”. John Wiley Sons, Inc., 1963
- [46] Alexander Ya. Malkin; Avraam I. Isayev, ”**Rheology: concepts, methods, and applications**”. ChemTec Publishing, Toronto, Ontario M1E 1C6, Canada, 2006
- [47] www.physics.usyd.edu.au/super/life_sciences/PM/PM5.pdf
- [48] www.encyclo.co.uk/define/Bingham%20plastic
- [49] Analysis of non-Newtonian liquids using a microfluidic capillary viscometer Srivastava, Nimisha ; Burns, Mark A., ”**Analysis of non-Newtonian liquids using a microfluidic capillary viscometer**”, *Analytical Chemistry*, Vol. 78, n 5, pag.

1690-1696, March 1, 2006

- [50] R.E. Rosensweig, "**Ferrohydrodynamics**". Mineola, New York: Dover Publication, INC, 1985
- [51] Analog Devices, "**Choosing Between Voltage Feedback (VFB) and Current Feedback (CFB) Op Amps**", MT-060 Tutorial, Rev.0, 10/08
- [52] Ron Mancini, "**Chapter 8: Current-Feedback Op Amp Analysis, Excerpted from Op Amps for Everyone**", Literature Number: SLOD006A, Texas Instruments Incorporated
- [53] Franco, Sergio, "**Design with operational amplifiers and analog integrated circuit** pag.347-396. Avenue of the Americas, New York, 10020: McGraw-Hill companies Inc., 2002.
- [54] Bruce Carter, "**Chapter 17: Circuit Board Layout Techniques SLOA089, Excerpted from Op Amps for Everyone**", Literature Number:SLOD006A, Texas Instruments Incorporated
- [55] M. Nikolo, "**Superconductivity: A guide to alternating current susceptibility measurements and alternating current susceptometer design**", *American Journal of Physics*, vol. 63, pp. 57-65, 1995.
- [56] Chen, D.-X.; Skumryev, V.; Bozzo, B., "**Calibration of ac and dc magnetometers with a Dy₂O₃ standard**", *Review of Scientific Instruments*, Vol. 82, n 4, April 2011
- [57] Chen, D.-X.; Skumryev, V., "**Calibration of low-temperature ac susceptometers with a copper cylinder standard**", *Review of Scientific Instruments*, Vol. 81, n 2, April 2010